

SHEAR ALIGNMENT OF PARTICLES DURING SPIN COATING

by

SYEDA SHARMIN HUSSAIN

A thesis submitted to the

Graduate School-New Brunswick

Rutgers, The State University of New Jersey

in partial fulfillment of the requirements

for the degree of

Master of Science

Graduate Program in Ceramics and Material Science and Engineering

written under the direction of

Prof. Dunbar P. Birnie, III

and approved by

New Brunswick, New Jersey

October, 2007

ABSTRACT OF THE THESIS

SHEAR ALIGNMENT OF PARTICLES DURING SPIN COATING

BY SYEDA SHARMIN HUSSAIN

Thesis Director:
Professor Dunbar P. Birnie, III

Spin coating is a process for applying uniform coatings to a wide variety of substrates. The final film thickness depends on viscosity, drying rate, percentage of solids, and surface tension and many of these influencing factors have been investigated. Our recent research has been focused on alignment of anisotropic particles being deposited by spin coating. One key aspect of spin coating is the shear forces that are experienced by the fluid before solvent evaporation takes over and freezes in a final particle arrangement. We have calculated the shear experienced by the particles during all stages of the process and tracked the fluid flow to determine the individual particle trajectories. A small fraction of fluid that starts near the center of the wafer contributes to the final coating while the majority of the fluid is flung off. From our calculations and associated measurements, it is evident that the particles away from the center of the wafer are more aligned toward the flow direction due to the higher shearing effect they experienced. Less alignment of particles is found near the center of the wafer as shear is significantly lower at the center. Experimental investigation has been performed to verify the numerical results. Alignment of the particles in the final coating can be advantageous for various optical, electrical and magnetic applications.

ACKNOWLEDGEMENT

First and foremost, I would like to thank my advisor Dr. Dunbar P. Birnie, III for his guidance and patience throughout the masters program. I am grateful for his encouragement and support as an advisor for helping me reach my goal. He is the best advisor and teacher I could have wished for. I would also like to thank my committee members Dr. Cosandey and Dr. Lehman for their valuable suggestions and time. I would like to thank Dr. Lai Qi, Judith Sorge, Sarika Phadke and Sukanya Murali for helpful discussions on my research at different stages of my graduate studies. I would like to thank my friends and officemate Beril and Milka for their support and wonderful company.

TABLE OF CONTENTS

| | |
|---|-----|
| Abstract of Thesis..... | ii |
| Acknowledgements..... | iii |
| Table of Contents..... | iv |
| List of Figures..... | vi |
| List of Tables..... | ix |
| 1 INTRODUCTION..... | 1 |
| 2 MATHEMATICAL FORMULATION..... | 6 |
| 3 NUMERICAL RESULTS..... | 10 |
| 4 INSTRUMENTATION..... | 20 |
| 4.1 SPIN COATER..... | 20 |
| 4.2 OPTICAL MICROSCOPE..... | 21 |
| 4.3 SCANNING ELECTRON MICROSCOPE..... | 22 |
| 4.4 X-RAY DIFFRACTION..... | 23 |
| 5 EXPERIMENTAL SECTION..... | 26 |
| 5.1 SYNTHESIS OF ZINCOXIDE NANORODS..... | 26 |
| 5.1.1 MATERIALS..... | 26 |
| 5.1.2 GROWTH PROCEDURE..... | 26 |
| 5.2 SYNTHESIS OF TITANIUM DIOXIDE NANORODS..... | 30 |
| 5.2.1 MATERIALS..... | 30 |
| 5.2.2 GROWTH PROCEDURES..... | 30 |
| 5.3 IRON OXIDE PARTICLES..... | 36 |
| 6 DATA ANALYSIS..... | 39 |

| | | |
|---|--------------------------------|----|
| 7 | DISCUSSION AND CONCLUSION..... | 45 |
| 7.1 | DISCUSSION..... | 45 |
| 7.2 | CONCLUSION..... | 48 |
| 8 | REFERENCE..... | 49 |
| APPENDIX A- Programs for the shear contour calculations and histogram | | |

LIST OF FIGURES

| | |
|--|----|
| Figure 1a Spin coating process..... | 1 |
| Figure 1b Fluid flow during spin coating..... | 1 |
| Figure 2.1 Cylindrical coordinate system..... | 6 |
| Figure 3.1: Transverse Shear aligning the particle along outward radial Flow (E.K. Franke and D. P. Birnie, III “Fibre Orientation during spin coating of composite solutions”)..... | 10 |
| Figure 3.2a Position tracking of 9 particles at same radial position with different fluid height at 2000 rpm for spinning time of 30 second and ethanol as fluid..... | 12 |
| Figure 3.2b Position tracking of 9 particles at same fluid height but different radial positions at 2000 rpm for spinning time of 30 seconds and ethanol as the fluid..... | 12 |
| Figure 3.3 Shear stress in radial direction, τ_r for 9 particles at different final fluid height for spinning speed of 2000rpm and spinning time of 2.885 second..... | 13 |
| Figure 3.4 Shear stress in axial direction, τ_z for 3 particles at final fluid thickness of 3 microns for spinning speed of 2000 rpm and spinning time of 2.885 second..... | 14 |
| Figure 3.5 Shear contour for final thickness ($h_{\text{cross-over}}$) of 3.73 microns spinning at 2000 rpm(total time for thinning is 1.864 second)..... | 15 |
| Figure 3.6 Shear contour plot for final thickness of 3 microns spinning at 2000 rpm (total time for thinning is 2.885 seconds)..... | 16 |
| Figure 3.7 Shear contour plot for final thickness of 1 micron spinning at 2000 rpm(total time for thinning is 25.986 seconds)..... | 16 |
| Figure 4.1.1 Spin coater model P6700 series..... | 20 |
| Figure 4.2.1 Axioskop 40 microscope..... | 22 |

| | |
|---|----|
| Figure 4.3.1a Field emission scanning electron microscope control panel (left) and auxiliary controls (right) at Rutgers University SEM laboratory (room no:CCR 107)..... | 23 |
| Figure 4.3.1b Filed emission scanning electron microscope chamber and detector system at Rutgers University SEM laboratory (room no: CCR 107)..... | 23 |
| Figure 4.4.1 Schematic of XRD system..... | 24 |
| Figure 4.4.2 Seimens Goniometer (D500) X-Ray Diffractometer..... | 25 |
| Figure 5.1.3 Locations on the wafer for the investigation..... | 28 |
| Figure 5.1.4: Image of Location 2 and the corresponding thesholded image using ImageJ...28 | |
| Figure 5.1.5 Image of location 1 and the corresponding histogram of particle alignment angles..... | 28 |
| Figure 5.1.6 Image of location 2 and the corresponding histogram of particle alignment angles..... | 29 |
| Figure 5.1.7 Image of location 3 and the corresponding histogram of particle alignment angles..... | 29 |
| Figure 5.2.3 XRD patterns of nanorods (A) without and (B) with acid autoclaving..... | 32 |
| Figure 5.2.4 The XRD pattern of TiO ₂ samples prepared from hydrothermal treatment of the nanotubes..... | 33 |
| Figure 5.2.5 SEM image of TiO ₂ nanotubes formed from basic hydrothermal treatment and acid wash..... | 34 |
| Figure 5.2.6 SEM image of TiO ₂ nanorods formed by hydrothermal treatment of nanotube suspension with pH value of 5.0..... | 35 |
| Figure 5.2.7 SEM images of TiO ₂ film on silicon wafer spun at a speed of 2000 rpm for 26 seconds..... | 36 |

| | |
|---|----|
| Figure 5.2.8 SEM images of TiO ₂ film on silicon wafer spun at a speed of 2000 rpm for 26 seconds at lower magnifications..... | 36 |
| Figure 5.3.1 SEM images of Iron oxide particles..... | 38 |
| Figure 5.3.2 SEM images of iron oxide particles..... | 38 |
| Figure 6.1 The different locations of the silicon wafer considered for the investigation..... | 39 |
| Figure 6.2: SEM image of iron oxide particles and the corresponding thresholded image.... | 40 |
| Figure 6.3 SEM image of Location 1 and the corresponding histogram of particle alignment angles..... | 41 |
| Figure 6.4 SEM image of Location 2 and the corresponding histogram of particle alignment angles..... | 42 |
| Figure 6.5 SEM image of Location 3 and the corresponding histogram of particle alignment angles..... | 42 |
| Figure 6.6 SEM image of Location 4 and the corresponding histogram of particle alignment angles..... | 43 |
| Figure 6.7 SEM image of Location 5 and the corresponding histogram of particle alignment angles..... | 43 |
| Figure 6.8: SEM Image of Location 6..... | 44 |
| Figure 7.1.1 Effect of radial position on the percentage of particles aligned along flow direction | 46 |
| Figure 7.1.2 Schematic of the edge effect..... | 47 |

LIST OF TABLE

| | |
|--|----|
| Table 3.1: Shear Integration Data..... | 18 |
|--|----|

Chapter 1

1. Introduction

Spin coating is a process for applying uniform coatings to wide variety of substrates. The formation of a thin, uniform layer of liquid on a flat rotating disk by centrifugal force is widely known as the spin-coating technique. This technique is widely used in the electronic industry to produce thin coating of polymeric photoresists for photolithography, sol-gel films for dielectric applications and planar structures for different optical applications. The figure 1a and 1b shows the spin coating process and fluid flow during spin coating.

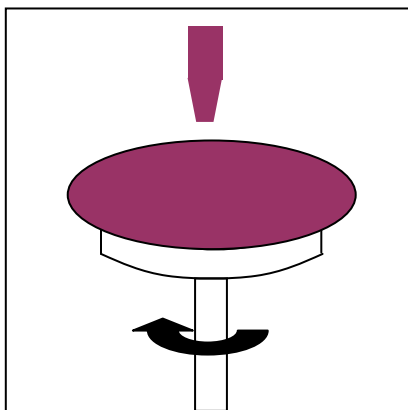


Figure 1a: Spin coating process.

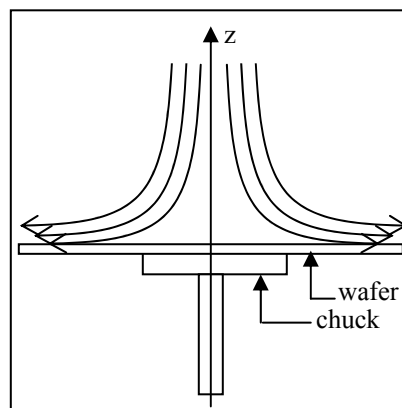


Figure 1b: Fluid flow during spin coating.

The final film thickness depends on viscosity, drying rate, percentage of solids, surface tension and other factors. Emslie, Bonner and Peck¹ developed an analytical model for the formation of a uniform layer for a Newtonian fluid. They showed that the final thickness is independent of the liquid profile at the beginning of rotation. The thickness decreases continuously with time as material is spun away. The evaporation rate of the solvent plays an important role in uniformity of the final coating. EBP¹ in their paper

illustrated the hydrodynamics of the spin coating process. The hydrodynamics are governed by the following two equations:

(i) conservation of mass :

$$\frac{\partial h}{\partial t} = -\frac{1}{r} \frac{\partial(rq)}{\partial r} \quad (1.1)$$

(ii) momentum equation (force balance i.e. during the spinning process the viscous force is balanced by the centrifugal force):

$$-\eta \frac{\partial^2 v}{\partial z^2} = \rho \omega r^2 \quad (1.2)$$

where, η is the viscosity, v is the radial velocity component, z is axial coordinate, q is the flow rate, h is the fluid height, ρ is the density, ω is the angular speed and r is the radius.

EBP¹¹ made the following assumptions to derive the momentum equation:

- a. The rotating plane is infinite in extent.
- b. The plane is horizontal, so that there is no radial gravitational component.
- c. The liquid layer is radially symmetric and so thin that differences in gravitational potential normal to the surface of the disk have negligible effect in distributing the liquid compared with the effect of centrifugal forces.
- d. The viscosity is independent of the rate of shear, i.e, the liquid is Newtonian.
- e. The liquid layer is everywhere so thin that shear resistance is appreciable only in horizontal plane.
- f. The radial velocity is everywhere so small that Coriolis forces may be neglected.

By integrating Equation (2) with two boundary condition, first, the no-slip condition of the fluid at the wafer i.e, $v = 0$ at $z = 0$; second is the shearing force is zero at the free

surface i.e, $\frac{\partial v}{\partial z} = 0$ at $z = h$, EBP¹¹ determined the total fluid thinning rate and derived a function for the fluid depth with time. The average thinning rate was found to be:

$$\frac{dh}{dt} = -2 \frac{\rho \omega^2}{3\eta} h^3 \quad (1.3)$$

Meyerhofer² investigated the effect of solvent evaporation on the film thickness. He modified the thinning rate equation by adding another term for thinning due to evaporation with the existing shear thinning term. This modified equation is stated below

$$\frac{dh}{dt} = -2 \frac{\rho \omega^2}{3\eta} h^3 - e \quad (1.4)$$

where, e is the evaporation rate.

Meyerhofer² assumed that the early stages of spin coating were entirely flow dominated, and later stages would be entirely evaporation dominated. This leads to the transition point at the condition where the evaporation rate and the viscous flow rate became equal. He also noted that the modified thinning rate equation leads to a cross-over from viscous flow controlled thinning at early stages of the process to evaporative controlled thinning near the end. He showed that the evaporation rate depends on vapor diffusion through the aerodynamic boundary layer above the wafer surface. In his model, the film thickness was evaluated for certain value of solvent evaporation rate and a specific relation between concentration and viscosity was considered. He expressed the film thickness as a function of spin speed, initial viscosity and evaporation rate.

The two factors governing the modified thinning rate equation are the flow constant K and the evaporation rate, e . The flow constant, K represents the combined effect of viscosity and spin speed. K is the system constant defined as

$$K = \frac{\rho\omega^2}{3\eta} \quad (1.5)$$

where, ρ is the fluid density, ω is the angular speed and η is the viscosity.

The evaporation rate e depends on rotation rate according to the following equation^{13,14}:

$$e = C\sqrt{\omega} \text{ micron /sec} \quad (1.6)$$

where, C is the proportionality constant and depends on the specific experimental conditions.

Birnie III and Manley³ showed the contribution of fluid flow and fluid evaporation to the total rate of thinning during spinning of a fluid on a silicon wafer. They applied laser interferometry to measure the shear flow and evaporation rate of fluid on the spinning wafer. They found that the flow behavior is consistent with the hydrodynamic equations given by EBP. They also show that Meyerhofer's modification to the EBP equation is required to account for evaporating fluids.

Our present research has been focused on alignment of anisotropic particles being deposited by spin coating. One key aspect of spin coating is the shear forces that are experienced by the fluid before solvent evaporation takes over and freezes in a final particle arrangement. Grasher and BirnieIII⁴ found that a small fraction of fluid that starts near the center of the wafer delivers the bulk of the final coating while the majority of the fluid is flung off. They developed a set of equations for calculating shear rate with respect to the radial and axial directions. They expressed the flow rate and the velocity component with respect to r and z as:

$$q = \int_0^z v_r dz = K(-0.5rz^3 + 1.5rz^2h) \quad (1.7)$$

$$v_r = \frac{\partial r}{\partial t} = 3Krz(h - 0.5z) \quad (1.8)$$

$$v_z = \frac{\partial z}{\partial t} = Kz^2(z - 3h) \quad (1.9)$$

where q is flow rate, z is the height within fluid as it flows, r is the radial position of a particle .

Film thickness h as stated in Equation (1.7) through (1.9) can be expressed as the following equation:

$$h = \frac{h_0}{\sqrt{1 + 4Kh_0^2 t}} \quad (1.10)$$

where, h_0 is film thickness at time zero and shows variation of fluid height with time.

Equations (1.8) and (1.9) give the radial and axial velocities of a volume element respectively, that can be determined from the position, height of the fluid and process constant. In chapter two, based on these equations we have calculated the cumulative shear (from equation 2.6) experienced by the particles during all stages of the spin coating process and tracked the fluid flow to determine the individual particle trajectories. An experimental investigation is also performed to confirm with the numerical results. Alignment of the particles in the final coating can be advantageous for various optical, electrical and magnetic applications.

Chapter 2

2. Mathematical Formulation

We considered a film of incompressible fluid on a rotating flat disk. A cylindrical coordinate system (r, θ, z) was used in the mathematical formulation. The disk rotates at an angular velocity ω about the z axis. The coordinate system for the spin coating process is shown below:

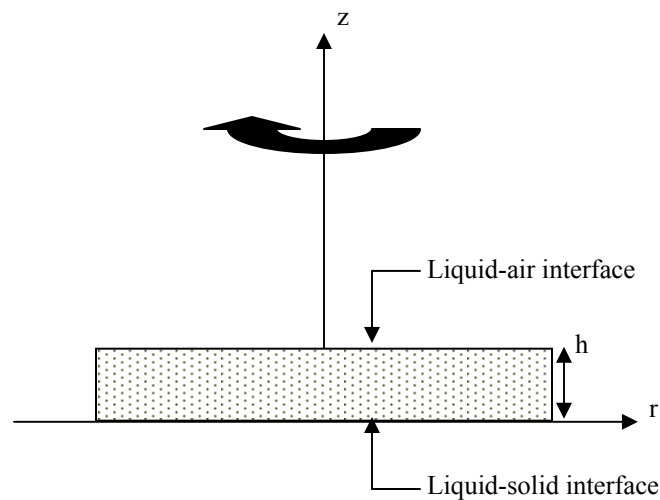


Figure 2.1: Cylindrical coordinate system.

The flow field is cylindrically symmetrical around the axis of rotation. Coriolis and surface forces were neglected. Pressure was assumed to be constant everywhere. The radius of the wafer was considered to be large in comparison to the thickness of the film, so that the edge effect can be neglected. The evaporation rate of the solvent is assumed to be constant.

The transition of thinning rate from shear to evaporation occurs when shear rate and evaporation rate are equal. From Equation (1.4) we can determine this transition point:

$$2Kh^3 = e \quad (2.1)$$

Taking evaporation rate and K as constant for simplification, from Equation (2.1), we get the following expression of cross over fluid height which corresponds to the fluid thickness when the structure gets effectively frozen:

$$h_{\text{cross-over}} = \left(\frac{e}{2K} \right)^{\frac{1}{3}} \quad (2.2)$$

Using $K = 9619.5 \times 10^6$ for rotational speed of 2000 rpm, ethanol as solvent (at 20° C) and $e = 1 \times 10^{-6}$ m/sec or 1 micron/sec from Birnie III and Manley³, the value of $h_{\text{cross-over}}$ is 3.73 micron. We will calculate cumulative shear for $h_{\text{cross-over}}$. Besides for $h_{\text{cross-over}}$, we will also calculate cumulative shear for the final fluid height h_f of 3 microns and 1 micron which corresponds to slower evaporation rate. The final fluid height h_f is the amount of fluid that remains on the wafer and creates the final coating. The initial fluid height is considered to be 100 micron for these three cases.

As the wafer rotates in its plane, it induces an axial air flow towards the wafer and creates a rotational motion at the liquid- air interface. The centrifugation causes the circulating liquid to move radially outward. The induced fluid shear based on equation 1.8 and 1.9 related to flow velocity field, has the following components:

(i) τ_r is the shear stress in radial direction,

$$\tau_r = \frac{\partial v_r}{\partial r} + \frac{\partial v_z}{\partial r}$$

$$\tau_r = 3Kz \left(\frac{h_0}{\sqrt{1 + 4Kh_0^2 t}} - 0.5z \right) \quad (2.3)$$

(ii) τ_z is the shear stress in axial direction,

$$\tau_z = \frac{\partial v_r}{\partial z} + \frac{\partial v_z}{\partial z}$$

$$\tau_z = 3K(r - 2z) \left(\frac{h_0}{\sqrt{1 + 4Kh_0^2 t}} \right) + 3Kz(z - r) \quad (2.4)$$

The shear stress τ_r and τ_z are function of r , z and t and effect of evaporation is negligible in early stages. The unit of shear rate is 1/second. The velocity gradient with depth is the dominant term in the shear rate equation (2.4). Since radial and axial coordinates r and z are function of time, their values can be calculated from the radial and axial velocity components (Appendix A, program II):

$$z = \int_0^z v_z dt = \int_0^z \frac{dz}{dt} dt = \int_0^z Kz^2 \left(z - 3 \left(\frac{h_0}{\sqrt{1 + 4Kh_0^2 t}} \right) \right) dz \quad (2.5)$$

Similarly,

$$r = \int_0^r v_r dt = \int_0^r \frac{dr}{dt} dt = \int_0^r 3Krz \left(\left(\frac{h_0}{\sqrt{1 + 4Kh_0^2 t}} \right) - 0.5z \right) dr \quad (2.6)$$

We calculated the cumulative shear experienced by the particles by integrating τ_z with respect to time t_f i.e. the time elapsed between dispensing the liquid on the substrate to the drying of the coating into static film (see program I in Appendix A.). In calculating

cumulative shear, we consider only the effect of shear with respect to z because, τ_z is the dominating component of shear during spin coating. The cumulative shear:

$$\int_0^{t_f} \tau_z dt = \int_0^{t_f} \left[3K(r - 2z) \left(\frac{h_0}{\sqrt{1 + 4Kh_0^2 t}} \right) + 3Kz(z - r) \right] dt \quad (2.7)$$

For three different final fluid heights of 1 micron, 3 microns and 3.73 microns, cumulative shear was calculated. The angular speed, time step and solvent were kept constant for the numerical calculation. The wafer diameter is taken to be 0.2 meter to disregard the edge effect. The initial condition is furnished by $h(t)$ at $t = 0$, that gives the initial distribution of the free liquid surface. The aim of this numerical calculation is to analyze the effect of shear on particle alignment for a certain initial thickness.

Chapter 3

3. Numerical Results

The numerical solution of Equations 1.8 and 1.9 were utilized to obtain a full tracking of the specific particle's spatial position during the spinning process ($r(t)$, $z(t)$), within a coating height, $h(t)$). We are considering anisotropic particles for numerical calculation because they are good indicator of fluid flow. Example of this tracking process is illustrated in Figures 3.2a and 3.2b. The position tracking is calculated for a spin time of 30 seconds.

When the fluid is flowing over the spinning substrate, the velocity gradient with depth creates a rotational force on the particles suspended in the solvent. The lower end of the particle experiences smaller radial motion than the upper end which is pushed out toward the flow direction rapidly. That is why anisotropic particles are good indication of shear alignment. Figure 3.1 is the schematic presentation of fluid flow field and its effect on shear alignment of anisotropic particles.

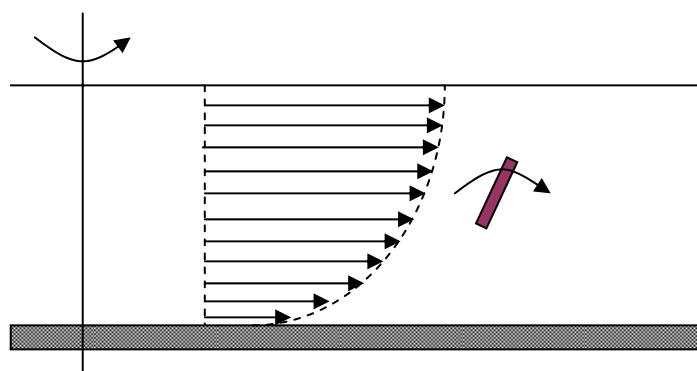


Figure 3.1: Transverse Shear aligning the particle along outward radial Flow (E.K. Franke and D. P. Birnie, III⁵ “Fibre Orientation during spin coating of composite solutions”).

As the fluid is flowing on the rotating substrate, due to the velocity gradient with depth the particle residing at higher fluid height has higher velocity and travels faster than a particle at lower fluid height at the same radial position (due to the velocity gradient). Thus the retention of the particle on the wafer depends on the initial location of the particle within the fluid body. From Figures 3.2a and 3.2b, it is evident that a particle further away from the wafer surface has greater possibility of being flung off. Consequently, it is more likely for the particles near the center of the wafer to contribute to the final coating.

An iterative solution procedure (see program II in Appendix A) is used to obtain the numerical solution of the nonlinear Equations (1.8) and (1.9) stated in Chapter 1 with the initial condition, $h(t) = h_0 = 100$ micron at $t = 0$ second (corresponding to uniform initial distribution). The finite flow domain $(0, r_d)$ is segmented into n intervals of step size Δr with nodes $r_1=0, r_2, r_3, \dots, r_n = r_d$. The time required to reach the final fluid thickness i.e. the time between dispensing the liquid on the wafer and attaining the fluid thickness that dries due to evaporation t_{final} is divided into 300 nodes with time interval of $\Delta t = \frac{t_{\text{final}}}{300}$.

For our calculation ethanol was considered as a representative solvent with viscosity and density at 20°C of 1.2 centi poise and 0.789 gm/cm^3 respectively.

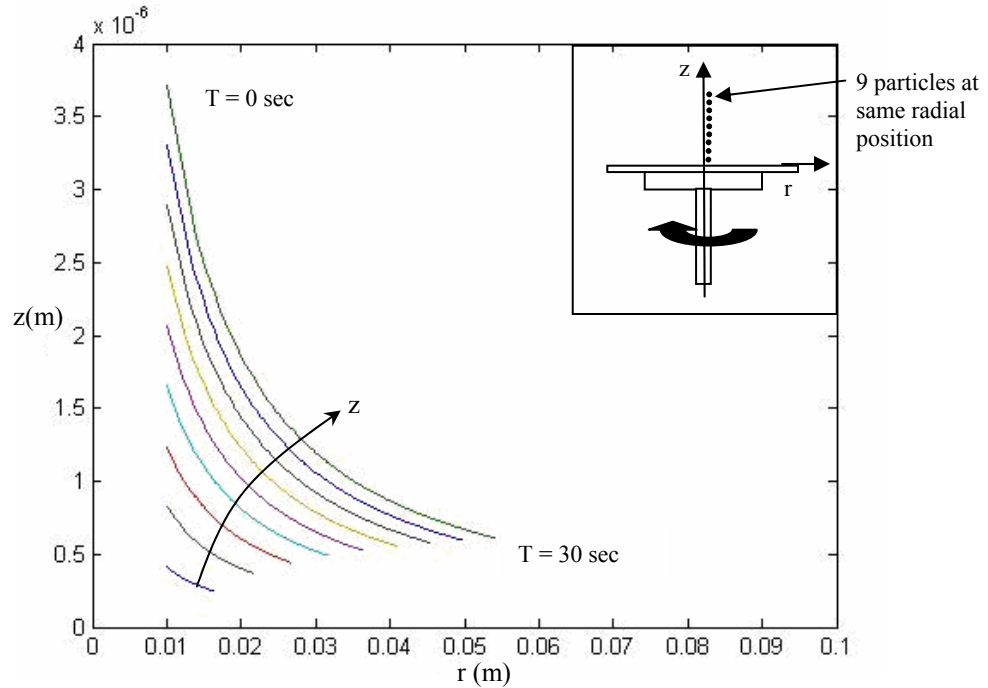


Figure 3.2a: Position tracking of 9 particles at same radial position with different fluid height, at 2000 rpm for spinning time of 30 sec and ethanol as fluid.

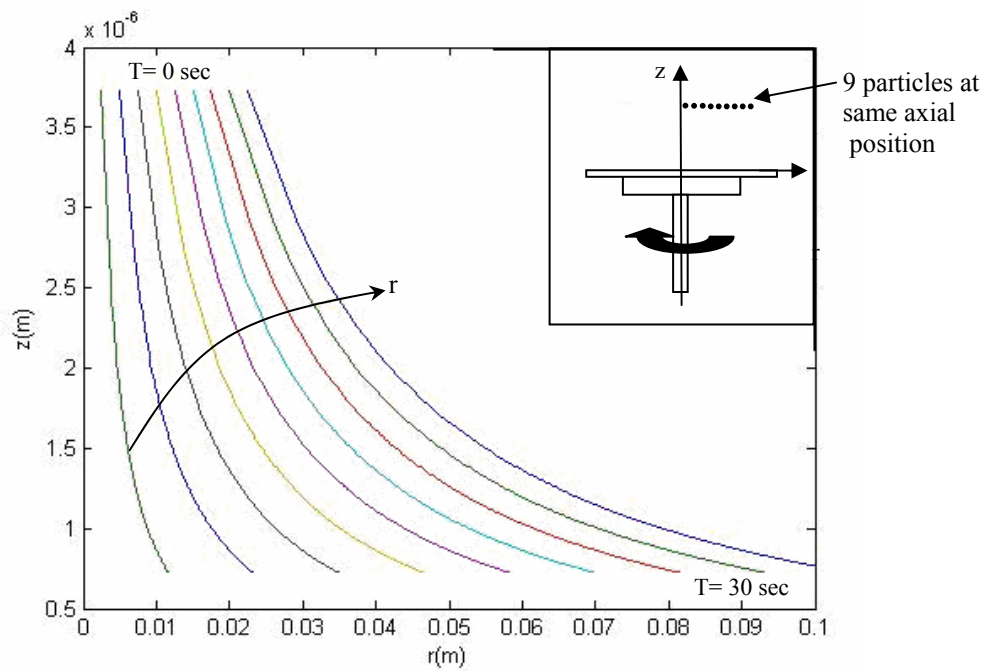


Figure 3.2b: Position tracking of 9 particles at same fluid height but different radial positions at 2000 rpm for spinning time of 30 sec and ethanol as the fluid.

The shear stress in radial direction is significantly smaller than that in axial direction. The shear in radial direction, τ_r , demonstrates the effect of fluid height on the particles in radial direction. Since τ_r is a function of axial position only, for any radial position of the particles, τ_r increases with increase of z (fluid height). Particles at higher z values in the final film would experience greater shear in the r direction. Shear stress in radial direction, τ_r , as function of z is shown in Figure 3.2 for 9 particles at different final fluid height ranging from $h_f = 0.3$ to 3 microns and for spin speed of 2000 rpm. Particle at higher z value, have higher velocity in r direction and those near the surface due to no slip condition have negligible or almost zero velocity. Subsequently, the change of radial velocity with respect to r is greater away from the surface. The plot of τ_r in Figure 3.3 illustrates this physical situation.

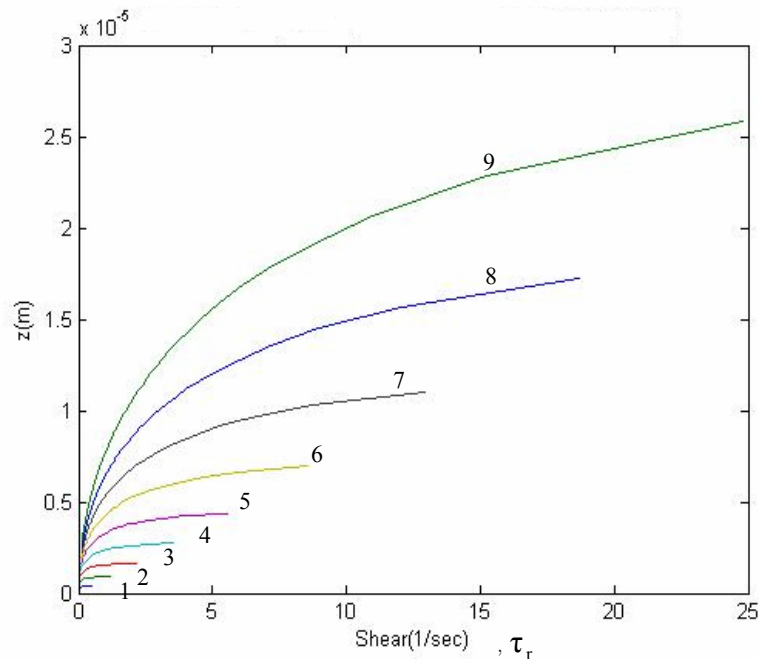


Figure 3.3: Shear stress in radial direction, τ_r , for 9 particles at different final fluid height for spinning speed of 2000 rpm and spinning time of 2.89 sec.

Since the shear stress in axial direction, τ_z is function of $r(t)$ and $z(t)$, the time evolution of axial shear is shown in a 3D grid pattern. The shear in axial direction τ_z was back calculated for three particles that are frozen in the final coating occupying different fluid heights at same radial position. When the wafer rotates, the particles embedded in the moving fluid experience shear τ_z due to the velocity gradient from the wafer to the free surface. As the fluid thickness on the wafer becomes thinner, the effect of shear on the particles lowers dramatically i.e. shear in axial direction τ_z decreases as the fluid height decreases during spinning. The shear rate with respect to depth is shown in Figure 3.4 for the three particles.

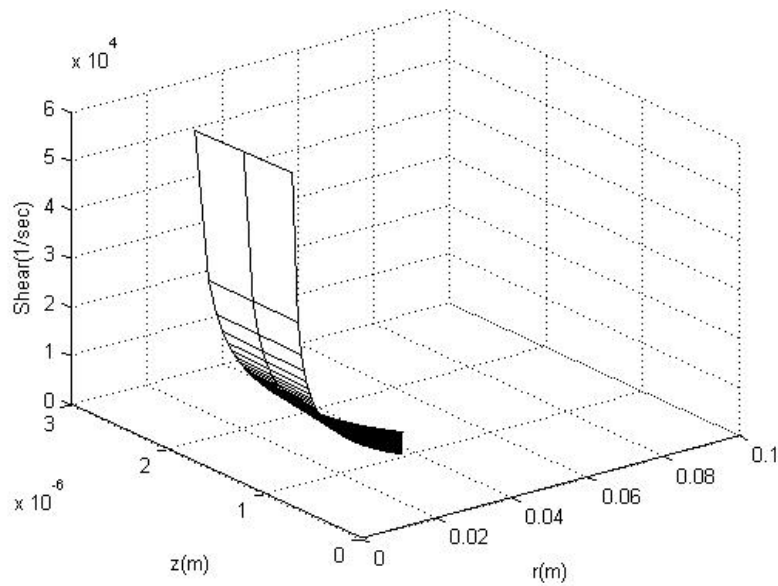


Figure 3.4: Shear Stress in axial direction, τ_z for 3 particles at final fluid thickness of 3 microns for spinning speed of 2000 rpm and spinning time of 2.885 sec.

From our shear rate calculation, it is evident that shear with respect to z is 1000 times larger than shear with respect to r . So particles get aligned along flow direction is mainly due to τ_z . The cumulative shear that the individual particle experiences as they flow

during a complete spinning run is calculated according to the Equation (2.6). The time is integrated from a fluid height associated with the initial dispense of fluid to the top surface of the wafer up to the point when the fluid reaches a chosen thickness (cumulative shear is calculated for three different final fluid height: 3.73 micron, 3 micron and 1 micro and the corresponding evaporation rate decreases as the final fluid height decreases) where it will start to dried by evaporation in to a static film and thus freezing the particles into their final location. The calculation illustrates that the particles further distant from the center of the wafer i.e. at the circumference of the wafer experience largest shear. Subsequently particles residing at higher fluid height have higher velocity and experience more shear. Due to $f(r)$, particles away from the center of the wafer tend to be more aligned to the flow direction than those at the center. Figures 3.4, 3.5 and 3.6 show this variation of shear with location on the substrate.

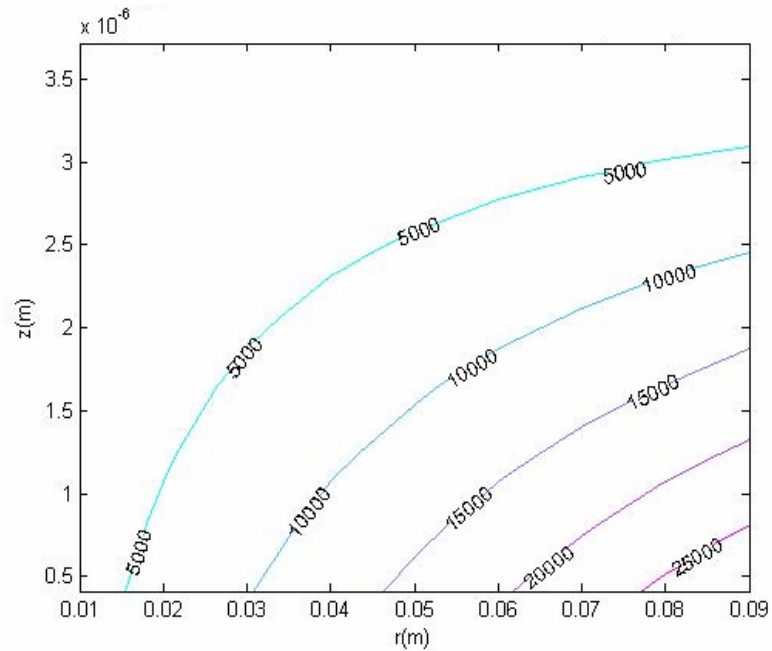


Figure 3.5: Shear contour plot for final thickness ($h_{\text{cross-over}}$) of 3.73 microns spinning at 2000 rpm (total time for thinning is 1.86 sec).

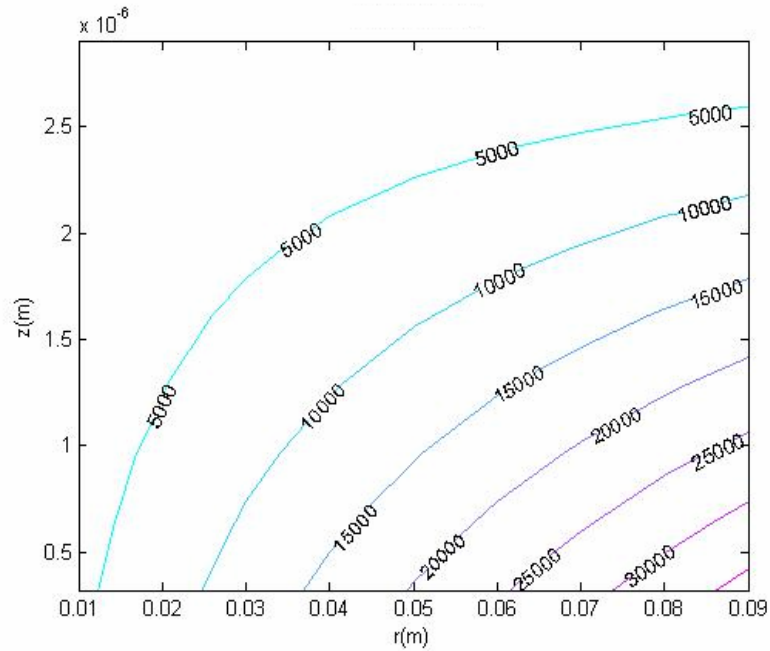


Figure 3.6: Shear contour plot for final thickness of 3 microns spinning at 2000 rpm (total time for thinning is 2.88 sec).

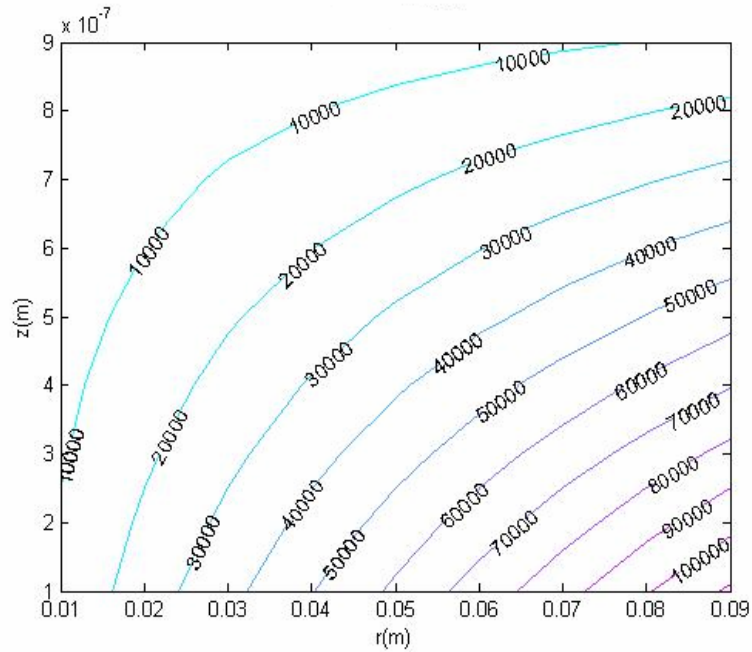


Figure 3.7: Shear contour plot for final thickness of 1 microns spinning at 2000 rpm (total time for thinning is 25.98 sec).

The particles near the center experience low shear due to smaller $f(r)$ and their orientation is effected by Brownian motion rather than fluid flow. Therefore, it is more likely for the particles near the center to remain unoriented, resulting in poor alignment to flow direction. The alignment of the particles depends significantly on the shear experienced by them i.e. the more shear, more aligned the particles are. From the shear integration data in Table 3.1 for $h_f = 3.73$ micron, we can see that the particles having thicker fluid layer above them experience more shear and shear reaches maximum as particles move toward the edge of the wafer.

Table.3.1. Shear Integration Data for final fluid height of $h_{\text{cross-over}}$:

| z (μ m) | r (m) | | | | | | | | |
|----------------|---------|---------|---------|----------|----------|----------|----------|----------|----------|
| | 0.01 | 0.02 | 0.03 | 0.04 | 0.05 | 0.06 | 0.07 | 0.08 | 0.09 |
| 0.41 | 3243.55 | 6487.42 | 9731.29 | 12975.16 | 16219.03 | 19462.9 | 22706.77 | 25950.64 | 29194.51 |
| 0.83 | 2767.81 | 5536.31 | 8304.8 | 11073.29 | 13841.79 | 16610.28 | 19378.78 | 22147.27 | 24915.77 |
| 1.24 | 2314.83 | 4630.75 | 6946.66 | 9262.57 | 11578.49 | 13894.4 | 16210.32 | 18526.23 | 20842.15 |
| 1.65 | 1884.76 | 3771.05 | 5657.34 | 7543.63 | 9429.93 | 11316.22 | 13202.51 | 15088.8 | 16975.09 |
| 2.07 | 1477.42 | 2956.86 | 4436.31 | 5915.75 | 7395.19 | 8874.64 | 10354.09 | 11833.53 | 13312.98 |
| 2.48 | 1092.04 | 2186.66 | 3281.28 | 4375.89 | 5470.51 | 6565.12 | 7659.74 | 8754.36 | 9848.97 |
| 2.89 | 726.91 | 1456.94 | 2186.98 | 2917.02 | 3647.06 | 4377.09 | 5107.14 | 5837.17 | 6567.21 |
| 3.30 | 378.62 | 760.875 | 1143.13 | 1525.38 | 1907.64 | 2289.89 | 2672.15 | 3054.40 | 3436.66 |
| 3.72 | 41.43 | 86.8029 | 132.18 | 177.55 | 222.92 | 268.29 | 313.67 | 359.044 | 404.42 |

The numerical results reveal that the alignment of the particles during spin coating is greatly influenced by the fluid shear along the flow direction. Since only a very small fraction of the total fluid (fluid near the center of the wafer and that close to the wafer surface) contributes to the final film thickness, while the rest is spun away, shear alignment is sensitive to final fluid thickness. The particles that reside at the outer skirt of the wafer experience more shear and have more alignment toward the flow direction. Poor alignment of particles is found near the center due to lower shear.

In addition to this theoretical analysis, an experimental investigation of flow alignment is performed. Well dispersed and high aspect ratio anisotropic particles are excellent candidates for testing this effect. They act as markers of coating flow alignment effects during spin coating.

Chapter 4

4. Instrumentation

The Instruments used for the experimental investigations were (i) Spin Coater (ii) Optical Microscope (iii) Scanning Electron Microscope, and (iv) X-ray Diffractometer. A brief description of these instruments is stated in this chapter.

4.1 Spin coater

The Spin Coater (P6700 series⁶) used for the thin coating is manufactured by Specialty Coating Systems. The precision coating systems are capable of executing thirty fully-

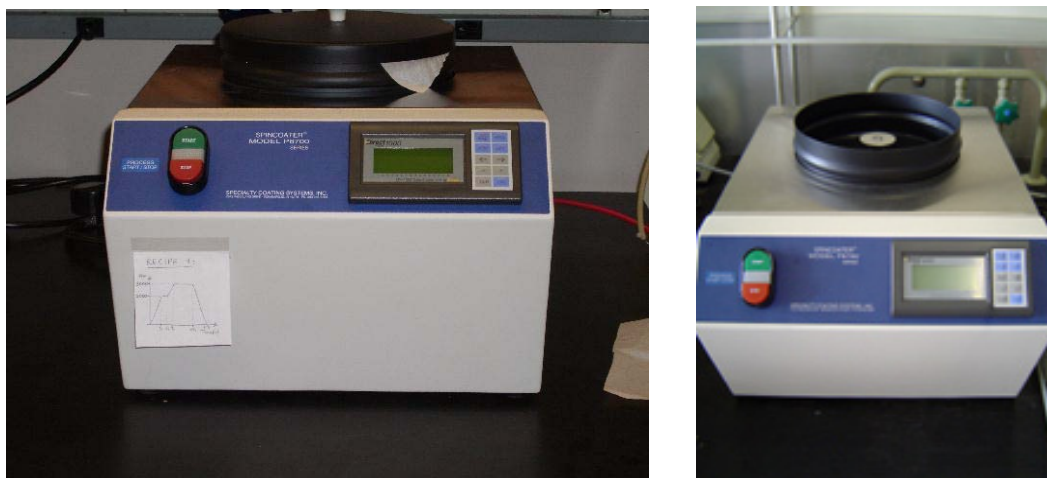


Figure 4.1.1: Spin Coater Model P6700 series (CCR 207).

automated, user-determined coating sequences under the supervision of a programmable logic controller. Each coating recipe consists of multiple ramp up, hold and ramp down steps in the range of 100-8000 rpm. Acceleration and deceleration rates are computer-calculated based on the desired profile. The P6700 series⁶ models include a simple keypad for programming and operation, and a user interface screen for display of process parameters. The unit is capable of handling a variety of shapes and substrate sizes up to

10 inches in diameter. The chuck is CS Type and used to hold a thin, planar surfaced substrate such as silicon, glass, or germanium on a spinning shaft for high rpm. The Spin Coater used in the investigation is shown in Figure 4.1.1.

There are four distinct stages to the spin coating process. The first stage is the deposition of the coating fluid onto the wafer or substrate. The second stage is when the substrate is accelerated up to its final, desired, rotation speed. During the third stage, the substrate is spinning at a constant rate and fluid viscous forces dominate fluid thinning behavior. In the fourth stage, the substrate is spinning at a constant rate and solvent evaporation dominates the coating thinning behavior. Stage 3 (flow controlled) and Stage 4 (evaporation controlled) are the two stages that have the most impact on final coating thickness⁷.

4.2 Optical Microscope

Axioskop 40 Microscope manufactured by Carl Zeiss and a digital camera are used to take image of particles. The microscope was an upright transmitted light microscope with three objective lens choices: 2.5X, 10X and 50X. The camera attached with the microscope is Spot Insight Firewire. The Spot Advanced software was used to take the images. Axioskop 40 Microscope used in the experimentation is shown in Figure 4.2.1.



Figure 4.2.1: Axioskop 40 microscope⁸. (CARL ZEISS) (CCR 234)

4.3 Scanning Electron Microscope (SEM)

The morphology of the coatings have also been examined from the images taken by the Field Emission Scanning Electron Microscope. The FESEM model is LEO- ZEISS GEMINI 982. The Scanning Electron Microscope is composed of the following four independent systems : (i) Vacuum System, (ii) the Probe Forming System, (iii) Scanning System, and (iv) the Detector System. Different parts of the LEO-ZEISS GEMINI 982 model are shown in Figure 4.3.1.



Figure 4.3.1a: Field Emission Scanning Electron Microscope control panel (left) and auxiliary controls (right) at Rutgers University SEM laboratory (Room No: CCR 107).



Figure 4.3.1b: Field Emission Scanning Electron Microscope chamber and detector system at Rutgers University SEM laboratory (Room No: CCR 107).

4.4 X-Ray Diffraction

TiO₂ Nanorods were characterized by X-Ray powder diffraction (XRD) using a Seimens

Goniometer (D500) X-Ray Diffractometer with Cu K α radiation ($\lambda = 0.154$ nm) at a scan rate of $1.2^\circ \text{ min}^{-1}$. The data were collected for scattering angles (2θ) ranging from 5 degree to 70 degree. Data collection was performed using the MDI "DataScan" software application.

The Siemens D500 powder diffractometer is a theta-theta configured goniometer that permits automated collection of intensity versus scattering angle scans. Data reduction schemes include unit cell determination, pattern indexing, and precision lattice parameter determination. Crystalline compounds are identified through the use MDI automation and analysis package with MDI Jade version 8.0 database of standard diffraction patterns. Schematic diagram of the XRD system is shown in Figure 4.4.1.

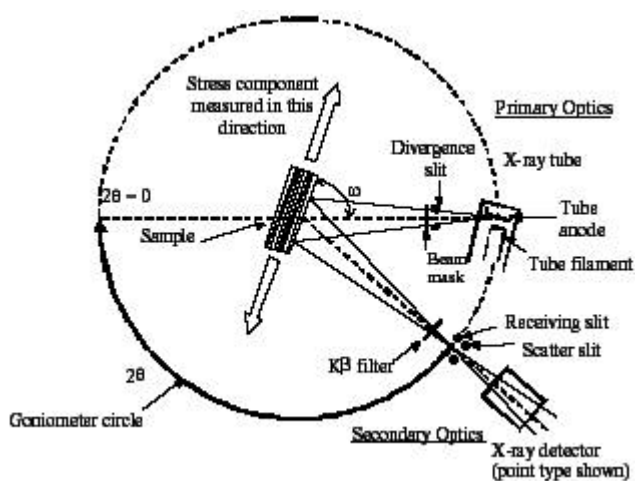


Figure 4.4.1: Schematic of XRD system⁹

The Siemens D500 powder diffractometer is shown in Figure 4.4.2.



Figure 4.4.2: Siemens Goniometer (D500) X-Ray Diffractometer¹⁰ (CCR 115)

Chapter 5

5. Experimental Section

An experimental investigation was performed to compare the numerical findings. Anisotropic particles are excellent candidate for our experiment. They act as markers of coating flow alignment effects during spin coating. The following anisotropic particles: ZnO nano rods, TiO₂ (anatase) nanorods and iron oxide nanorods were the three choices for the experimental investigation. The synthesis process followed in making the zinc oxide and titania nanorods are illustrated in the following subsections.

5.1 Synthesis of ZnO Nanorods

One dimensional ZnO nanostructure is used in nanodevices such as light-emitting diodes, field effect transistors and solar cells. ZnO nanorods can be grown by a low temperature hydrothermal process using an aqueous solution that contains zinc salt and an organic amine. The detailed procedure for the hydrothermal growth is explained by Cui et al¹¹.

5.1.1 Materials

The chemicals used in this study were zinc nitrate hexahydrate powder ($\text{Zn}(\text{NO}_3)_2 \cdot 6\text{H}_2\text{O}$) which was purchased from Fisher Scientific, USA , hexamethylenetetramine ($\text{C}_6\text{H}_{12}\text{N}_4$) purchased from Sigma Aldrich and distilled water .

5.1.2 Growth Procedure

Growth solution was prepared by dissolving a calculated amount (0.6gm) of zinc nitrate hexahydrate in 200 ml of distilled water to make 0.01M solution. Consecutively hexamethylenetetramine (0.2857 gm) was added to the zinc nitrate aqueous solution. The concentration of hexamethylenetetramine is also 0.01M. Hydrothermal ZnO nanorod

growth was carried out in a plastic beaker with a glass cover. The growth temperature was selected in the range of 60 to 90°C and the typical growth time was 6 hour. After the growth, the solution was decanted. The white solution left at the bottom was centrifuged at 3000rpm for 2 minutes to remove the solvent from the solute. Then the ZnO nanorods were washed with distilled water repeatedly until all the solvent was removed from the solute. After rinsing the ZnO paste is dispersed in ethanol. A dilute solution (10% v/v) of ZnO was prepared.

The zinc oxide solution was then deposited on silicon wafer. The wafer was spun at 2000 rpm for 30 seconds. Images of the wafer were taken using Optical microscope (Axioskop 40) and a digital camera. We investigated the shear alignment of the particles by processing the images using ImageJ software. ImageJ software identified individual particles based on brightness and contrast. Thresholding of each image is done manually according to the available lighting condition. Different parameters of each thresholded particle were quantified including the position(x ,y), angle of orientation (with respect to horizontal axis), aspect ratio, perimeter and area. Clustered and interacting particles were eliminated by considering particles with aspect ratios between 2.5 to 5.0 and histogram (see program III in Appendix A) of particle alignment angles is plotted.

The ZnO nanorods that were synthesized for the study were approximately 8 micron in length. Even though ZnO grows naturally as nanorods (hexagonal crystal structure), it is difficult to get well isolated particles. The regions on the wafer that were investigated are shown in the Figure 5.1.3. Figure 5.1.4 is showing location 2 of the wafer and the corresponding thresholded image using ImageJ software. For histogram, only particles with aspect ratio of 2.5 to 5.5 are considered to avoid clustered particles.

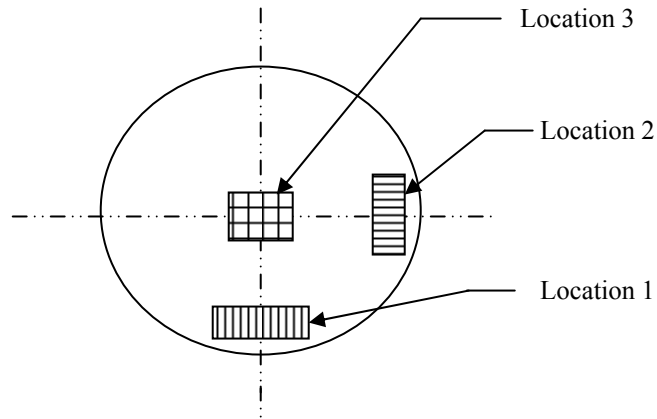


Figure 5.1.3: Locations on the wafer for the investigation.

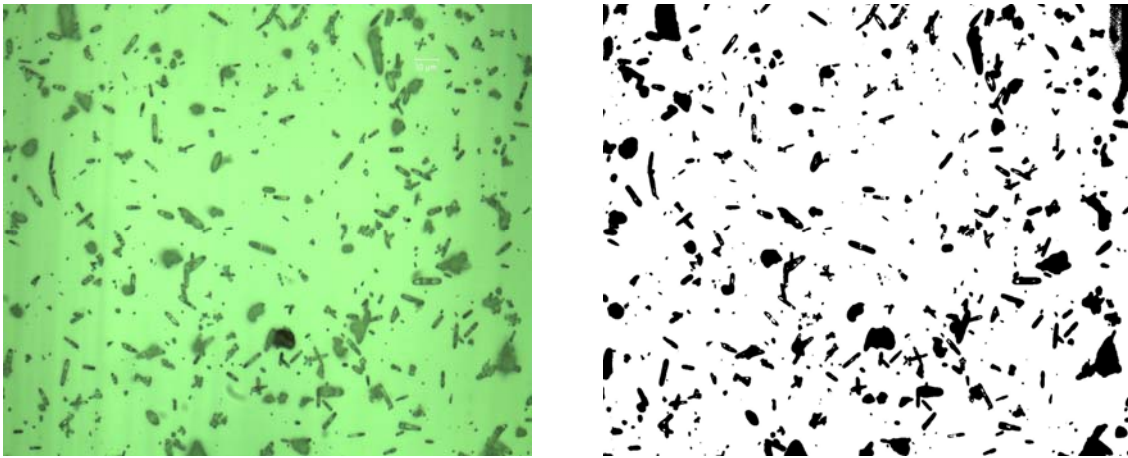


Figure 5.1.4 : Image of Location 2 and the corresponding thresholded image using ImageJ.

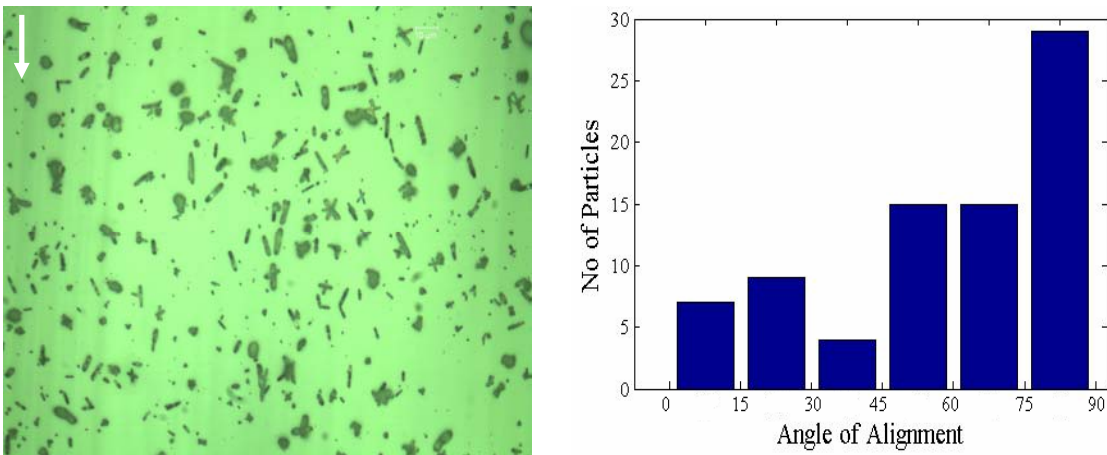


Figure 5.1.5: Image of Location 1 and the corresponding histogram of particle alignment angles. The white arrow in the image of Location 1 is showing the flow direction.

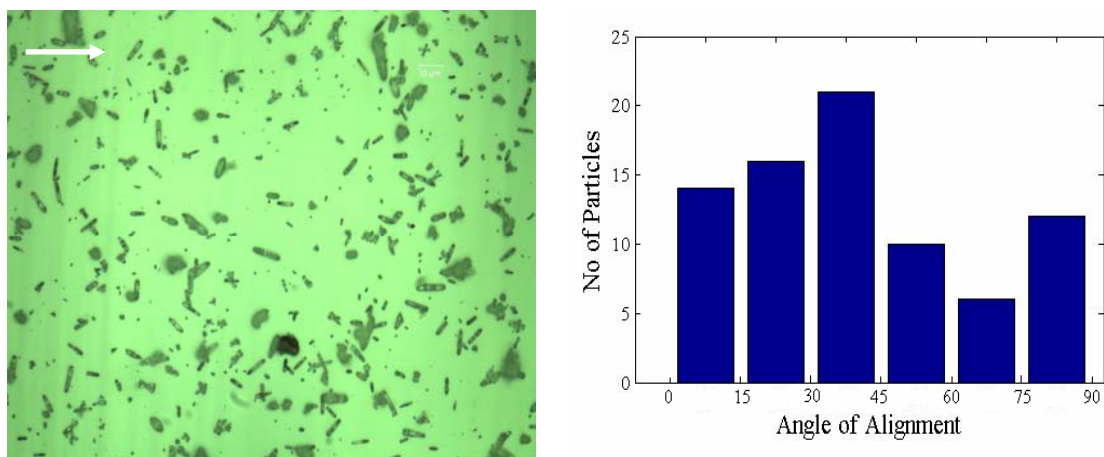


Figure 5.1.6: Image of Location 2 and the corresponding histogram of particle alignment angles. The white arrow in the image of Location 2 is showing the flow direction.

The shear alignment of the zinc oxide nanorods is not very pronounced at Location 1 and 2. This is illustrated in Figure 5.1.4. Similarly Figure 5.1.5 shows poor alignment effect due to the presence of too many clustered particles.

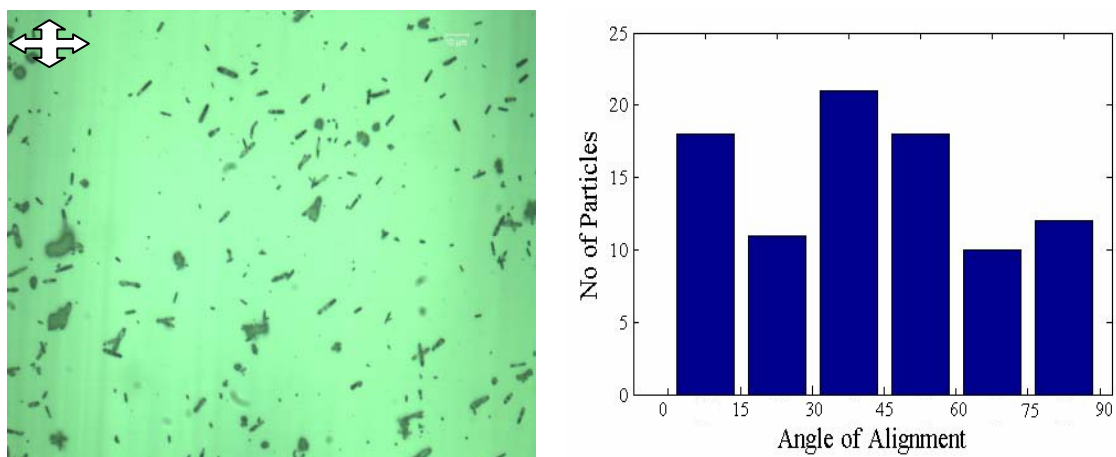


Figure 5.1.7: Image of Location 3 and the corresponding histogram of particle alignment angles. The white arrows in the image of Location 3 are showing the flow direction.

The Location 3 shows the nanorods at the center of the wafer. The effect of low shear is not prominent from this histogram.

5.2 Synthesis of TiO₂ Nanorods

Nanocrystalline TiO₂ is widely used in photoelectrochemical systems. Nanorods have large surface area available for dye absorption and therefore more absorption of photons compared to bulk material, helping to increase the efficiencies for solar cells. Nanotubes of TiO₂ can be derived from alkali treatment of TiO₂ nanoparticles under a basic condition¹². These nanotubes can be considered as precursor for the growth of 1D TiO₂ structures under a less basic or acidic condition.

5.2.1 Materials

All chemicals were of the highest purity available and were used as received without further purification. TiO₂ powder (P25, Degussa AG, Germany) which consists of about 30% rutile and 70% anatase. The primary particle size was approximately 21 nm. NaOH (97%, Sigma Aldrich) and HNO₃ (70%, Acros).

5.2.2 Growth Procedures

The synthesis procedure involved for making TiO₂ nanorods was outlined by Poudel¹² and Nian¹³. The synthesis was done in two steps: (i) hydrothermal growth of TiO₂ nanotubes in basic solution and (ii) hydrothermal growth of nanorods with TiO₂ nanotubes as the precursor in acid solution. The growth solution was prepared by mixing 1.5 gram of P25 powder with 84 ml of 10 M NaOH aqueous solution and stirred for 1 hour in a beaker. Then the solution was transferred into 100 ml autoclave (84% filling fraction) and autoclaved at 120° C for 30 hours. After the treatment, the precipitate was treated with 0.1 N HNO₃ solution for several times in order to reduce the pH of the solution. After the hydrothermal treatment, the pH of the solution was 12 (very basic). The acid wash was repeated until the pH of the nanotube solution reached 5.0. The suspension with a volume

of about 80 ml was subjected to hydrothermal treatment in the autoclave at 175° C for 48 hours. The resulting slurries were then collected and dispersed in distilled water. HNO₃ wash removes the electrostatic charge from the sheets and leading to the formation of nanotubes. Heating these nanotubes at 175° C for 48 hours in an acidic environment resulted in the formation of single-crystalline anatase nanorods with a specific crystal-elongation direction¹³. Nian and Teng explained the procedure in details in their paper.

The obtained samples were characterized by X-Ray powder diffraction (XRD) using a Seimens Goniometer (D500) X-Ray Diffractometer with Cu K α radiation ($\lambda = 0.154$ nm) at a scan rate of 1.2° min⁻¹. The data were collected for scattering angles (2θ) ranging between 5° and 70°. The microstructure was explored with a field emission scanning electron microscope (LEO- ZEISS GEMINI 982, operating at 5 KeV). Figure 5.2.3 shows the XRD pattern of the product obtained from hydrothermal treatment with and without acid autoclaving.

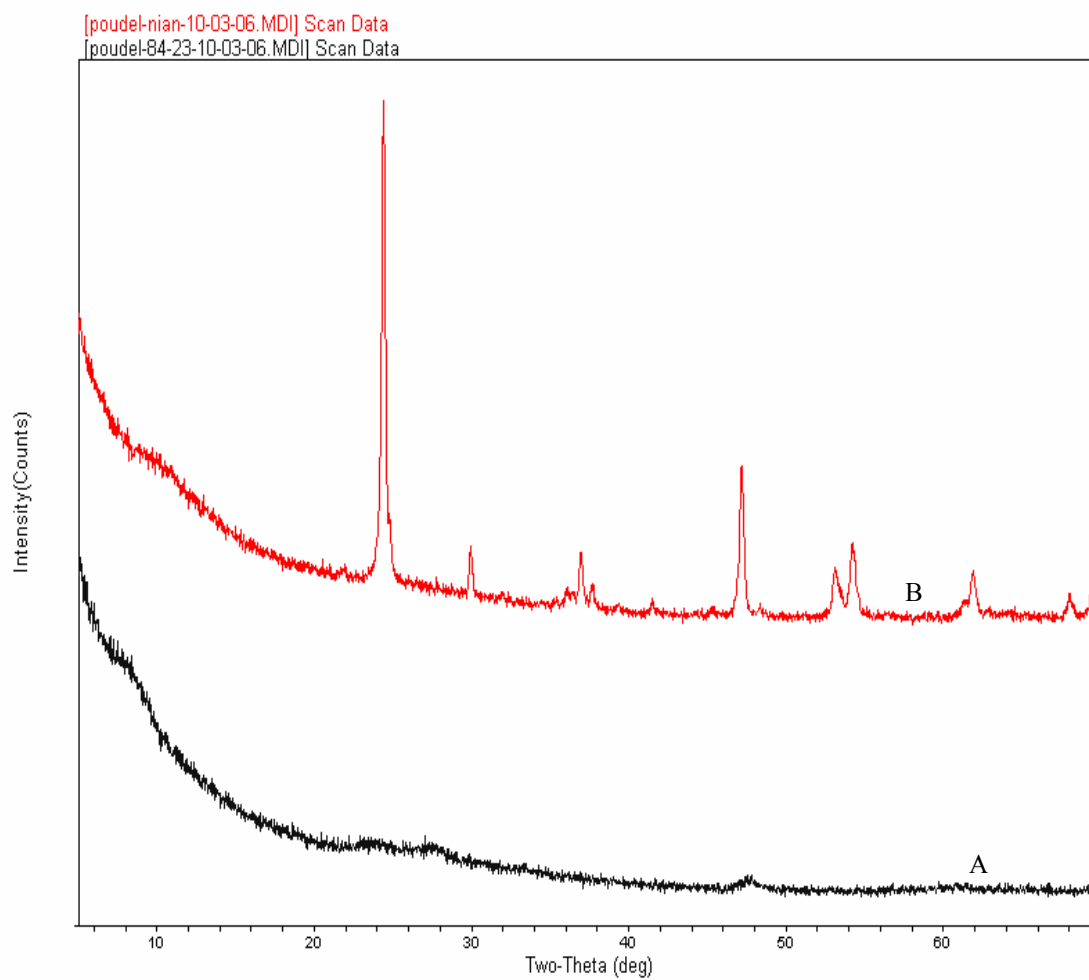


Figure 5.2.3: XRD patterns of nanorods (A) without and (B) with acid autoclaving.

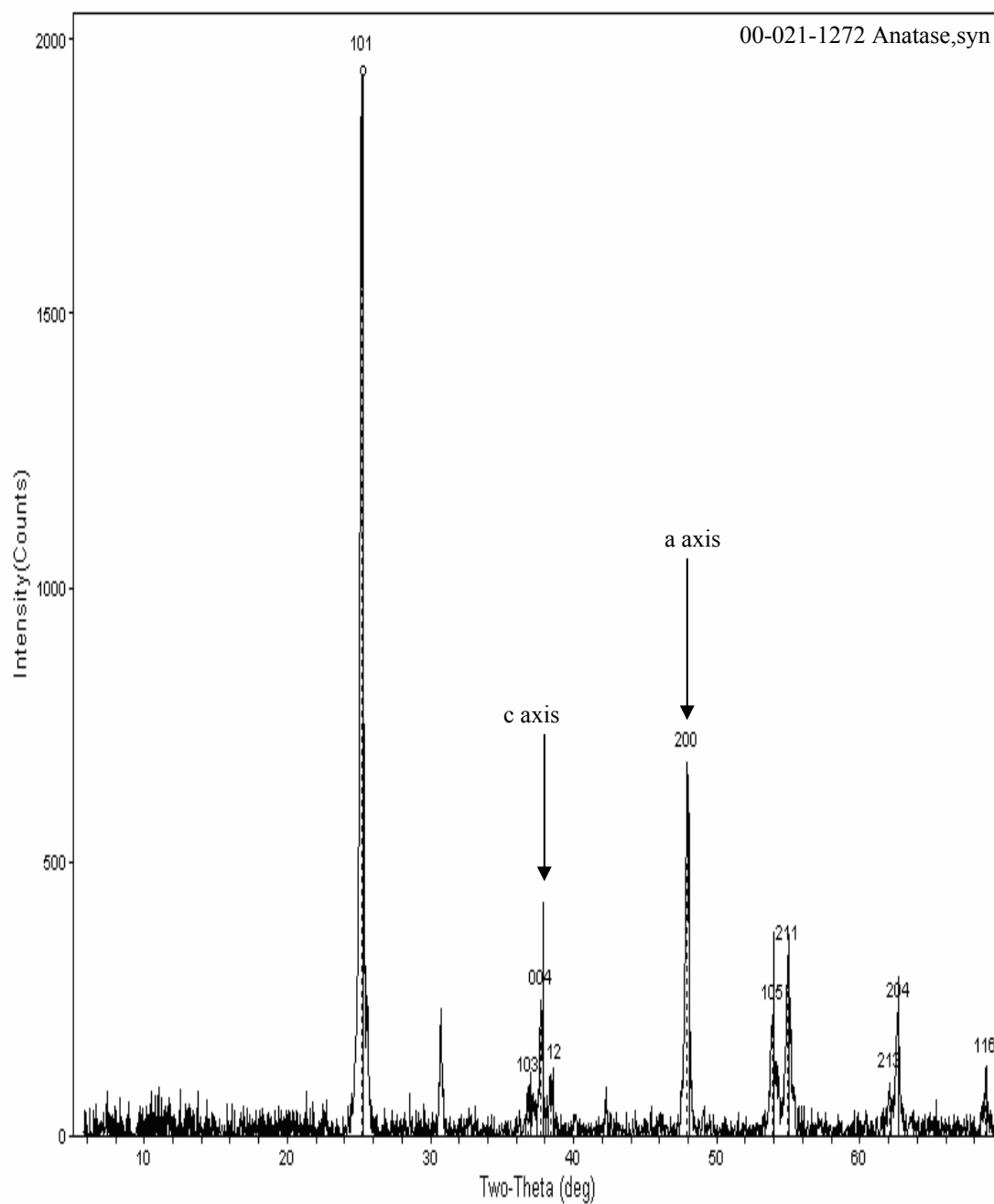


Figure 5.2.4: The XRD pattern of TiO₂ samples prepared from hydrothermal treatment of the nanotubes.

For the sample obtained with an acidic condition (pH=5.0), the peak positions are consistent with the standard diffraction pattern of anatase TiO_2 which is shown in Figure 5.2.4.

The morphology of the nanotube samples was examined using scanning electron microscope (SEM). The SEM image of the microstructure of TiO_2 nanotubes without acid treatment is shown in Figure 5.2.5.

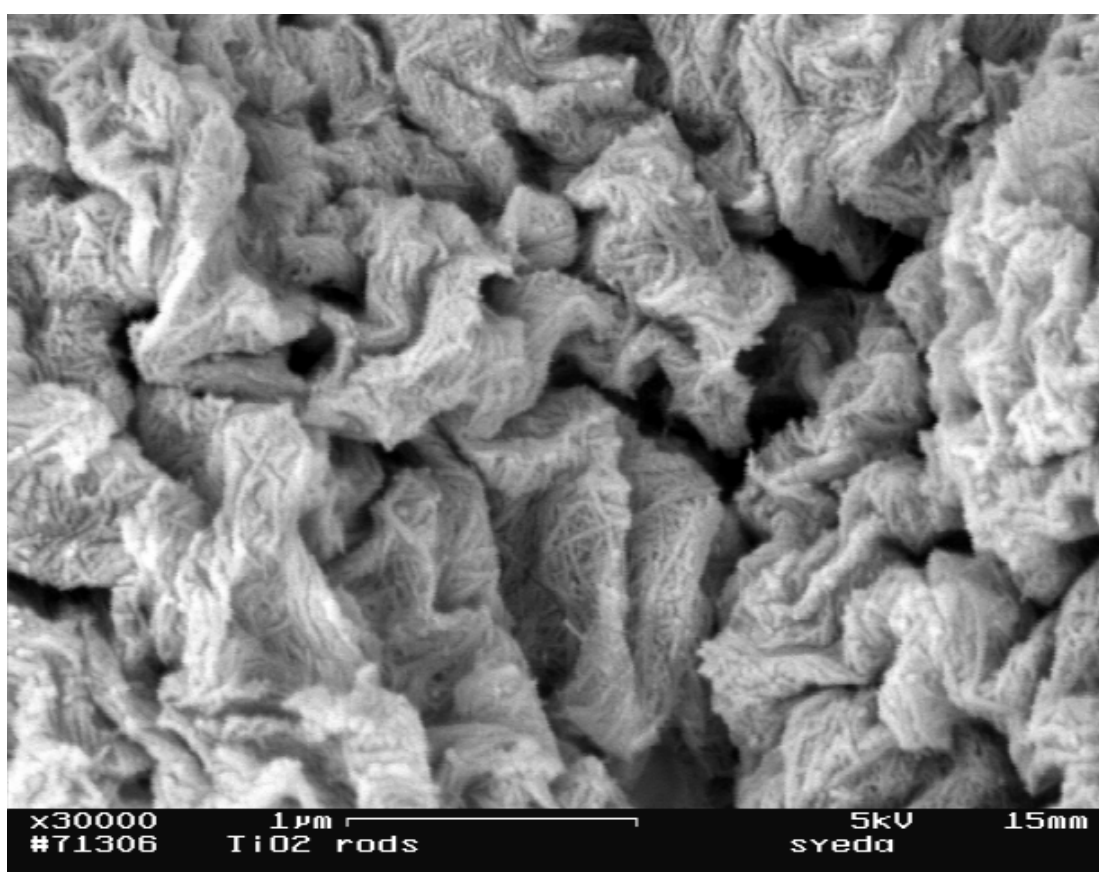


Figure 5.2.5: SEM image of TiO_2 formed from basic hydrothermal treatment and acid wash.

Figure 5.2.6 shows the SEM image of the TiO_2 particles obtained from the hydrothermal treatment of the nanotube suspensions under acidic conditions.

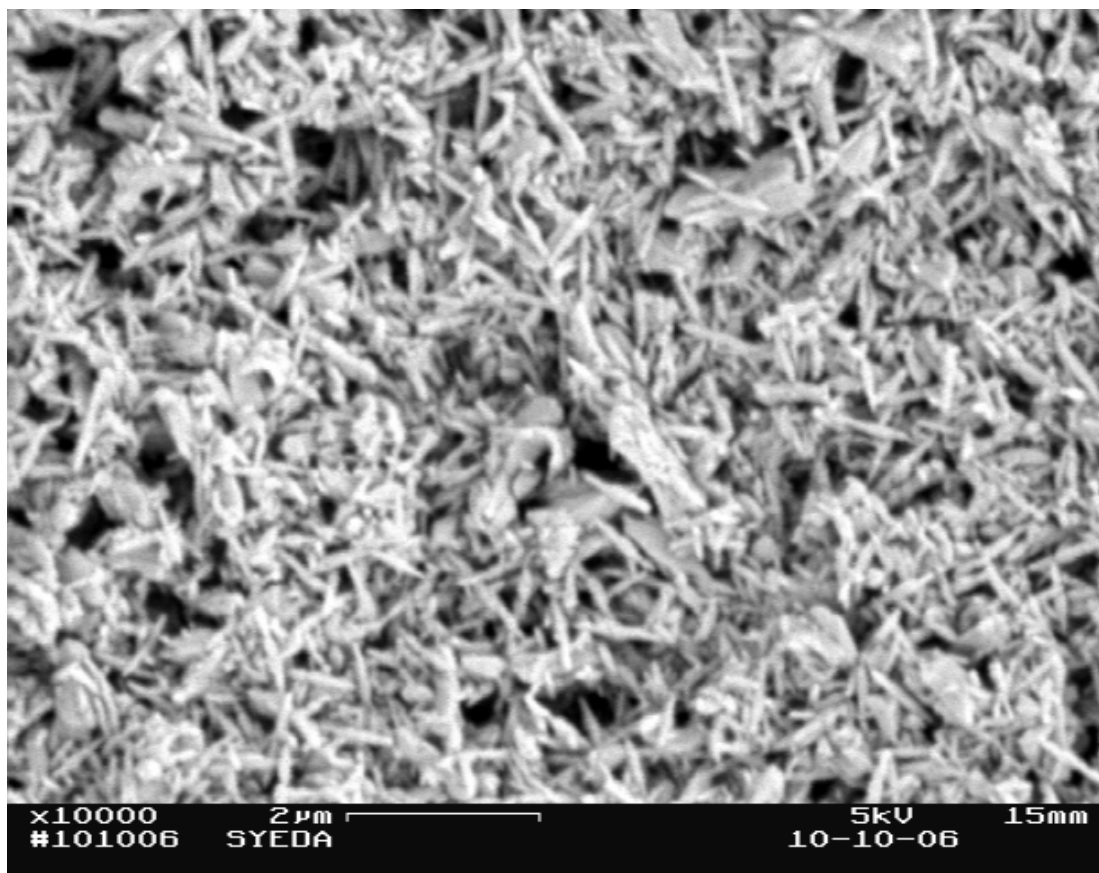


Figure 5.2.6: SEM image of TiO₂ nanorods formed hydrothermal treatment of nanotube suspensions with pH value of 5.0 .

The solution of TiO₂ nanorods was diluted with distilled water. The diluted solution of TiO₂ nanorods were dispensed on silicon wafer and spun at 2000 rpm for 26 seconds. The coating was not uniform and the TiO₂ particles remain clustered on the wafer. Excessive efforts were made to stabilize and disperse these particles but they remain clustered. So the TiO₂ nanorod solution did not produce the desired coating for investigating shear alignment of the particles. The SEM images shown in Figure 5.2.7 and Figure 5.2.8 show the clustered TiO₂ particles on the wafer.

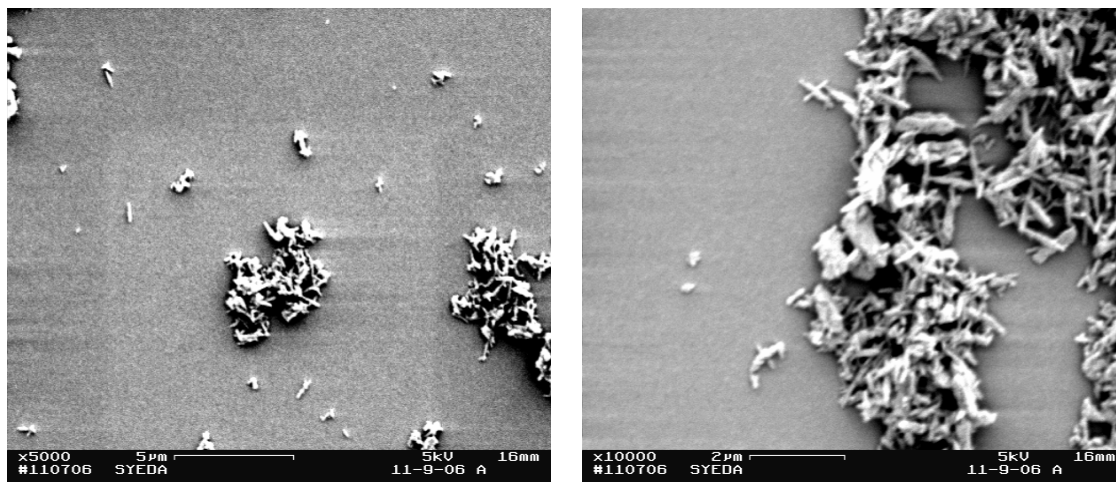


Figure 5.2.7: SEM images of TiO₂ film on silicon wafer spun at a speed of 2000 rpm for 26 seconds.

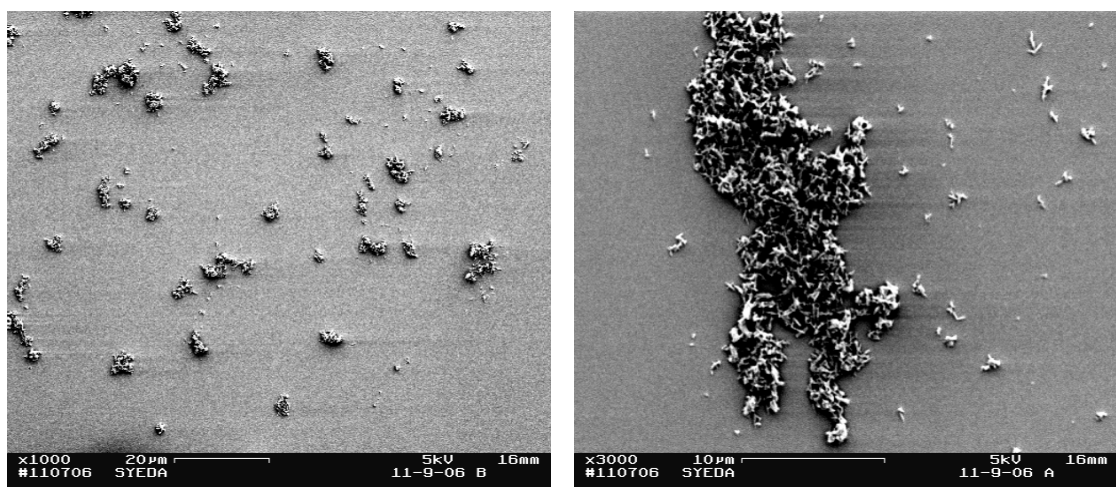


Figure 5.2.8: SEM images of TiO₂ film on silicon wafer spun at a speed of 2000 rpm for 26 seconds at lower magnifications.

5.3 Iron Oxide Particles

The anisotropic particles described in section 5.1 to 5.2 did not produce good coatings for the shear alignment investigation that we had designed. However, with iron oxide particles with non-magnetic hematite (Fe₂O₃) core we were more successful. These

particles were provided as a part of research collaboration with Dr. Chekesha Liddell's group, Department of Material Science and Engineering, Cornell University.

The particles were approximately 1.4 micron in length with aspect ratio of 2.8. These particles are peanut shaped and dispersed in deionized water (DIW). The viscosity of DIW is 0.9 centipoises at 25⁰ centigrade. Since the solution is dewetting the substrate, we treated the silicon wafer (2 inch in diameter).

The substrate is treated by applying a thin coating of polyvinyl alcohol (PVA) on the wafer. PVA act as an adhesive. The polymer solution is a 0.2 % PVA in distilled water. The polyvinyl alcohol which is solid at room temperature, dissolved in distilled water at an elevated temperature (near the boiling point) at a concentration of about 0.2%. The PVA solution was then dispensed on the wafer and spun at a speed of 2000 rpm for 26 seconds. The PVA coated wafer was air dried. The thickness of the PVA coating is approximately 43 nm. The thickness of the PVA coating was measured by spectroscopic ellipsometer (Jobin Yvon / Horiba).

The iron oxide solution was deposited on the PVA coated wafer in large enough quantity to cover the whole surface. Then the wafer was spun at a speed of 2000 rpm for 26 seconds. After deposition, the coating was air dried. We investigated the alignment of particles by taking scanning electron microscope (SEM) images at different locations of the silicon wafer at the same magnification. The morphology of the iron oxide particles is shown in Figure 5.3.1 and Figure 5.3.2.

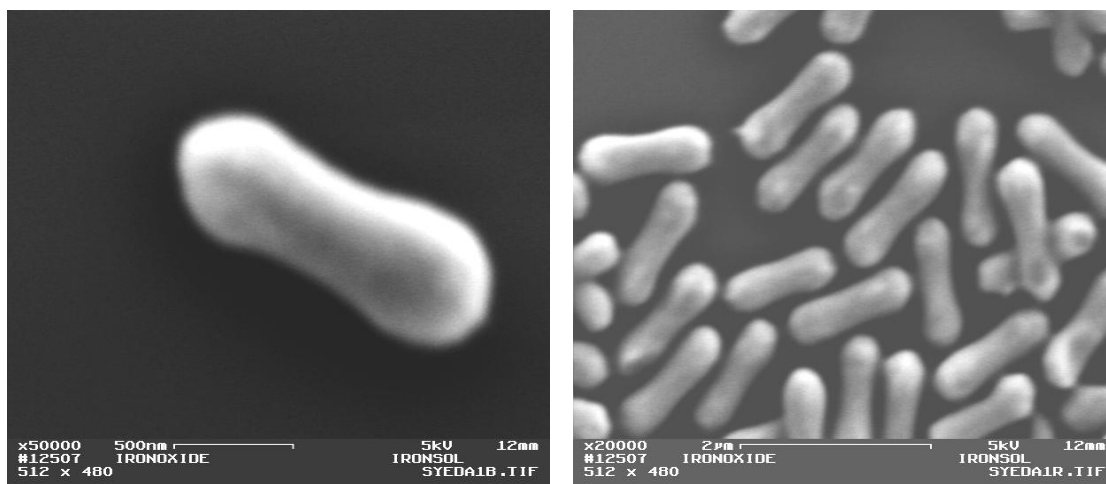


Figure 5.3.1: SEM images of Iron Oxide particles at various magnifications.

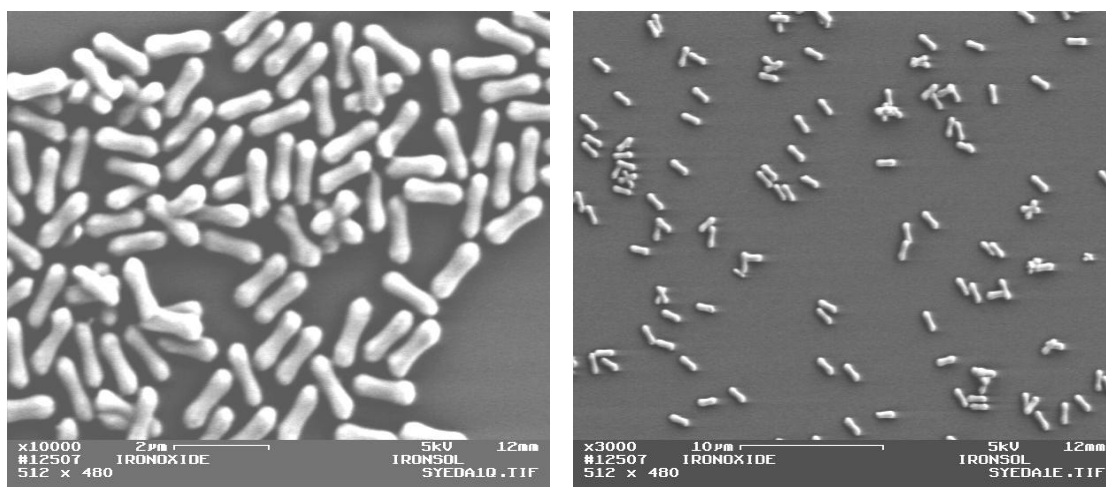


Figure 5.3.2: SEM images of Iron Oxide particles

Chapter 6

6. Data Analysis

The particle arrangement of each image is quantified by analyzing each particle's angle of orientation α_i , with the horizontal axis and its aspect ratio. For the particles in each region based on the radial distance from the center (shown in Figure 6.1), a histogram is plotted showing the distribution of angular deviation. We grouped the angles into 15° bins and the counts are plotted for this angular deviation. Franke and Birnie III⁵ investigated the effect of shear and stretching gradients on fiber orientation during spin coating of composite solution. In that investigation, the effect of evaporation is eliminated by using transparent oil as solvent. They found that for the fibers at same radial distance from the center, the largest fraction align themselves to within 15° of their ideal radial orientation and a very few had 75 to 90° deviation at the same radial distance.

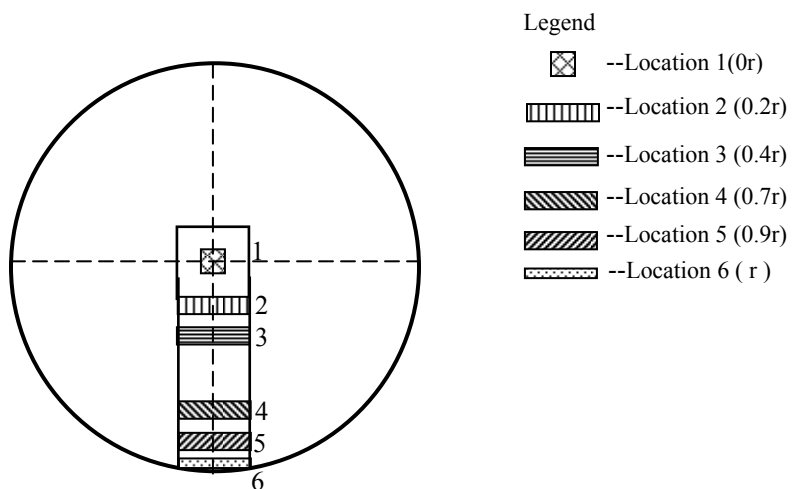


Figure 6.1: The different locations of the silicon wafer considered for the investigation.

Figure 6.2 shows SEM image of iron oxide particles and the corresponding thresholded image using ImageJ software.

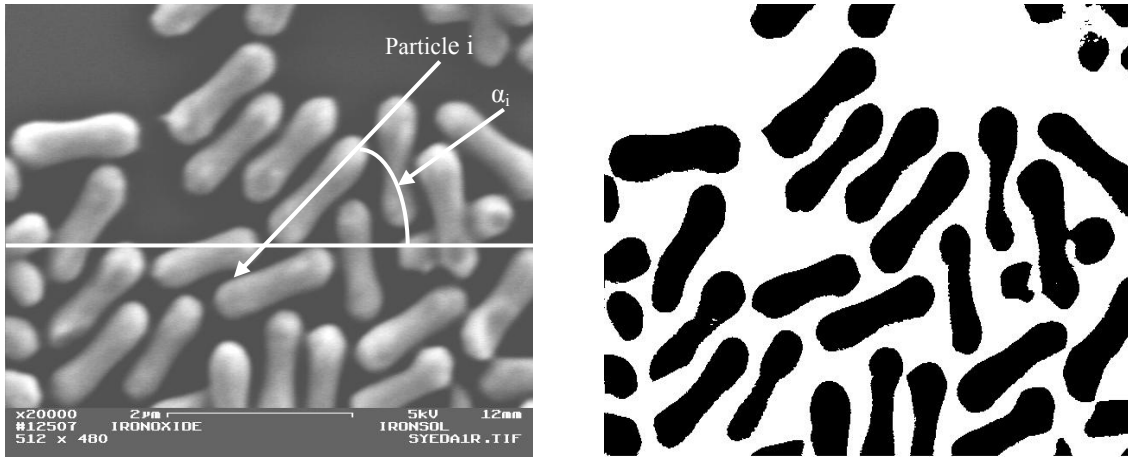


Figure 6.2: SEM image of iron oxide particles and the corresponding thresholded image.

The high cumulative shear that we calculated earlier is expected to contribute to the alignment of the rod shaped particles during the spin coating process. Since the flow is radially outward, the particles have a tendency to get aligned with the flow direction and this effect is enhanced toward the edge of the silicon wafer. From our calculations we found that the shear is low at the center and gradually increases toward the edge of the wafer. The particles at Location 1 shown in Figure 6.3 have higher concentration due to low radial velocity leading to more particle interaction. With increase of radial distance from the center, the radial velocity of the fluid becomes higher as we can see from the following equation of radial velocity of fluid at any point (r, θ, z) given by EBP¹:

$$v_r = \frac{\rho\omega^2 r z}{\eta} (h - 0.5z)$$

As a result, poor alignment effect is found at the center in comparison to other locations away from the center. Histogram of Figure 6.3 confirms this argument.

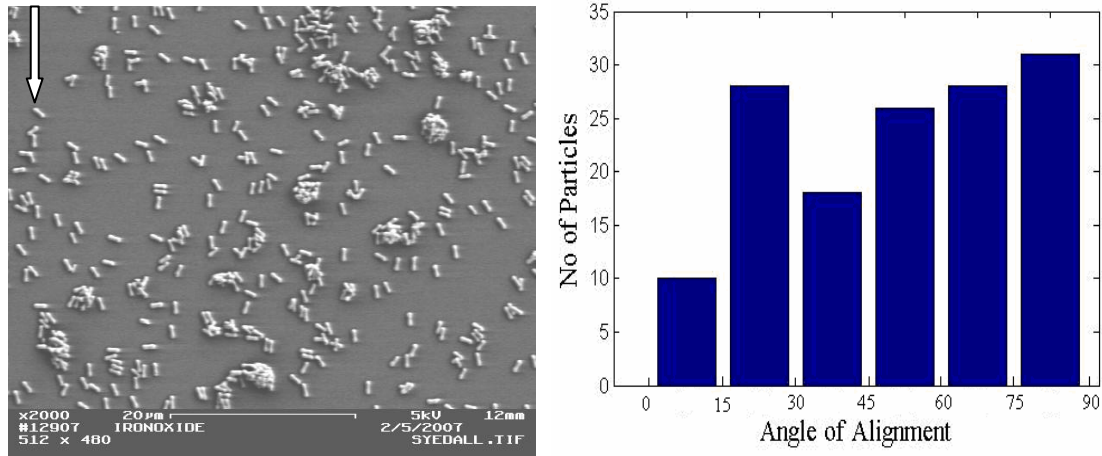


Figure 6.3: SEM Image of Location 1 and the corresponding histogram of particle alignment angles. The white arrow shows the flow direction.

The image of particles at Location 1 (Figure 6.3) shows the particles in ‘lying down’ position. The fluid which is in direct contact with the substrate has a zero velocity and the velocity of fluid gradually increases toward the top layer. This velocity gradient creates a rotational force on the particles suspended in the fluid. The lower end of the particle experiences less rotational motion than the upper end of the particle; the resulting motion difference forces the particle to a ‘lying down’ position that is aligned with the major shear force. When the fluid thickness reduces below the length of the particles, the particles have another motion constraint and are forced to lie down throughout randomly. This phenomenon was explained early by Franke and Birnie. Figures 6.4 and 6.5 show images of locations at greater radial distances from the center of the wafer. As we move away from the center, cumulative shear increases, more and more particles get flow aligned which is evident from the histograms of Figures 6.4 and 6.5.

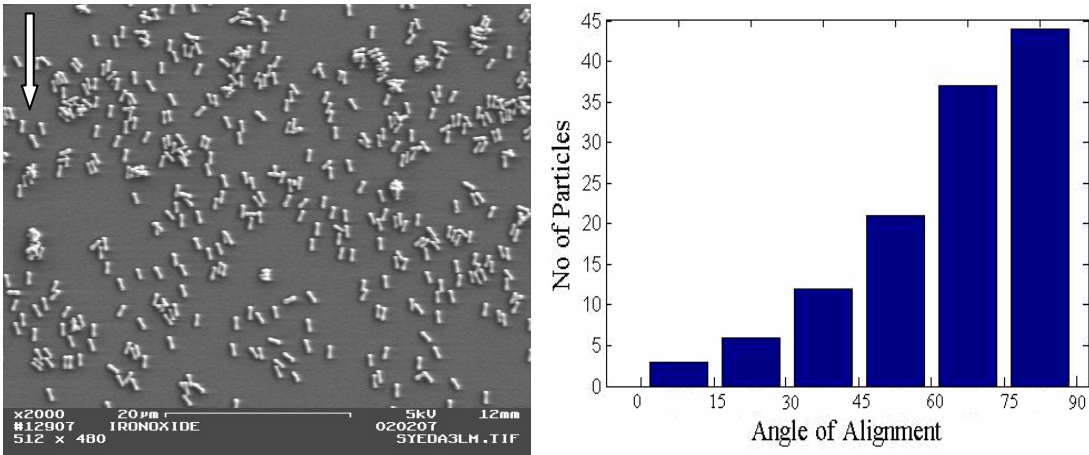


Figure 6.4: SEM Image of Location 2 and the corresponding histogram of particle alignment angles. The white arrow shows the flow direction.

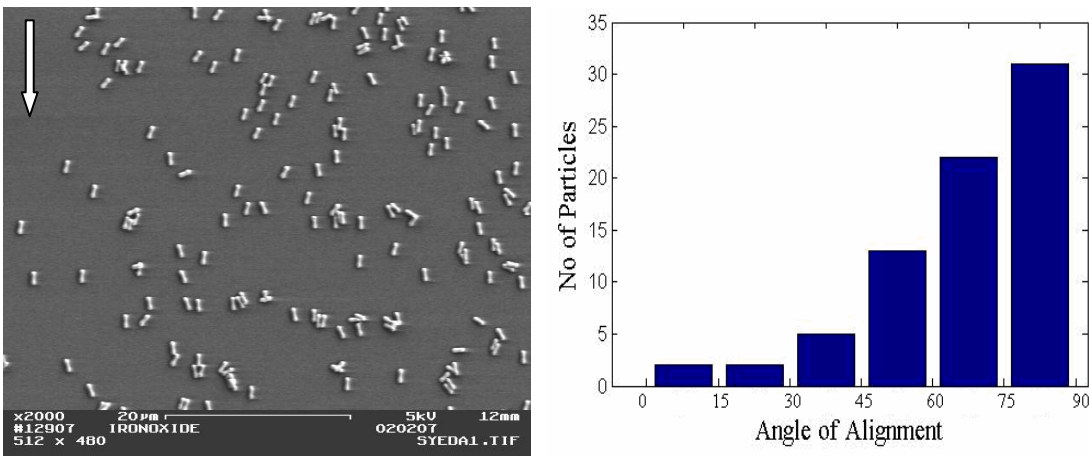


Figure 6.5: SEM Image of Location 3 and the corresponding histogram of particle alignment angles. The white arrow shows the flow direction.

Particles at the Location 4 are (i.e. further away from the center compared to Locations 2 and 3 as discussed earlier) shown in Figure 6.6. In this figure, the degree of flow alignment is even more pronounced. From the histogram we can see that largest fraction of the single particles are aligned along the angle ranging from 75 to 90°.

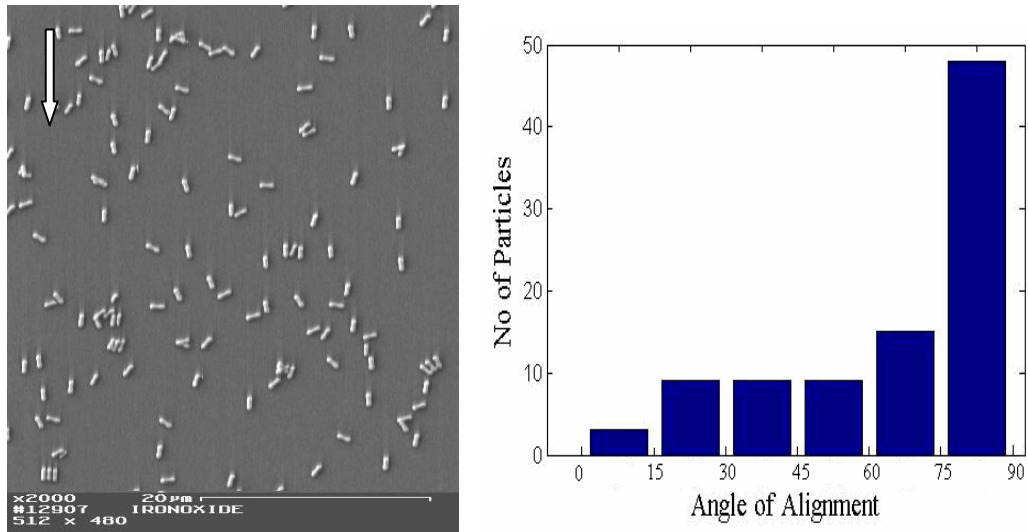


Figure 6.6: SEM Image of Location 4 and the corresponding histogram of particle alignment angles. The white arrow shows the flow direction.

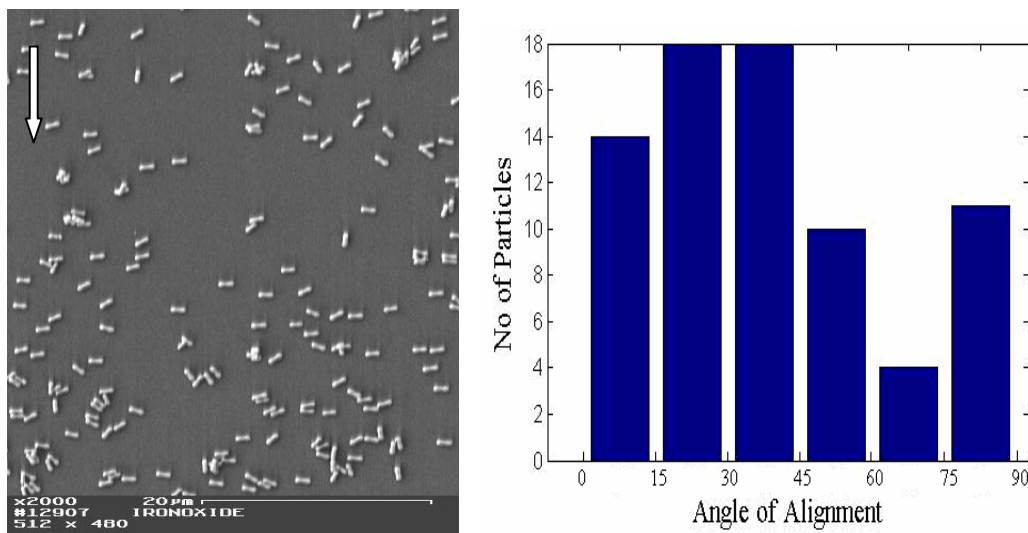


Figure 6.7: SEM Image of Location 5 and the corresponding histogram of particle alignment angles. The white arrow shows the flow direction.

Particles at the Location 5 (Figure 6.7) are at greater radial distance from the center than those at the Location 4. From Figure 6.7 it is evident that near the edge the shear alignment of particles is not very strong. Because near the edge, the flow dynamics is more complicated and also the edge effect plays an important role on the alignment of

particles. The alignment effect is not present at the edge of the wafer, as we can see from Figure 6.8. The particles seem to be stacked into a thicker film at the rim of the wafer. From this image it is evident that high shear due to the spinning has no effect on the near edge particles. A more complex process is involved at the edge of the wafer. Three overlapping images were taken at the same magnification and placed together to show the behavior at the edge. This figure shows the edge effect at the rim of the wafer.

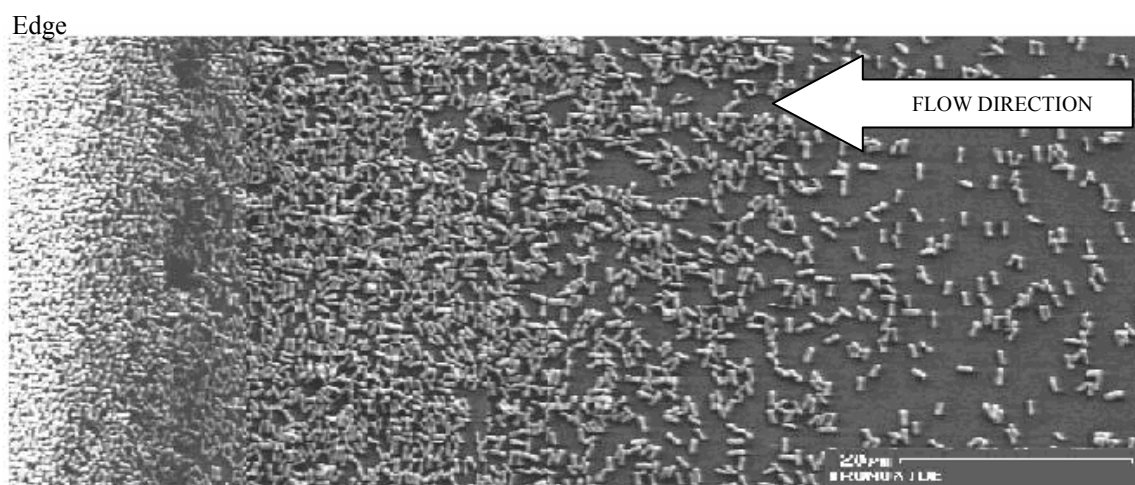


Figure 6.8: SEM Image of Location 6.

Chapter 7

7. Discussion and Conclusion

7.1 Discussion

The numerical results reveal that alignment of the particles during spin coating is could be influenced by the cumulative shear along the flow direction. The particles that end up further out on the outer skirt of the wafer experience more shear and have more alignment toward the flow direction. Poor alignment of particles is found near the center due to low shear.

Our experiments also show that there is a marked radial increase in alignment of the rods as we move further from the center of the wafer until we get to the edge bead. From the images of different locations of the wafer shown earlier, it is evident that the distributions of particles are not exactly radial. This is due to the initial random orientation of dispensed particles. A significant fraction of particles are found to have angular deviation greater than 15° from ideal radial direction. However, the overall particle distribution as shown by the histograms yield net alignment of particles along the radial directions due to the high cumulative shear. Because of the very high cumulative shear, a greater amount of alignment effect was expected than we have actually found in our investigation. This is mainly due to the fact that, the calculation does not account for the full 3D range of orientation effects and the full tumbling action that the particles experience during the flow. The experimental investigations also show that there is a marked radial increase in alignment of the peanut shaped particles as we move further from the center of the silicon wafer. Figure 7.1.1 shows the percentage of particles getting aligned along flow direction. This graph is based on the histograms of 5 locations

on the wafer shown in chapter 6. This finding is also consistent with the calculation showing higher shear at larger radius values.

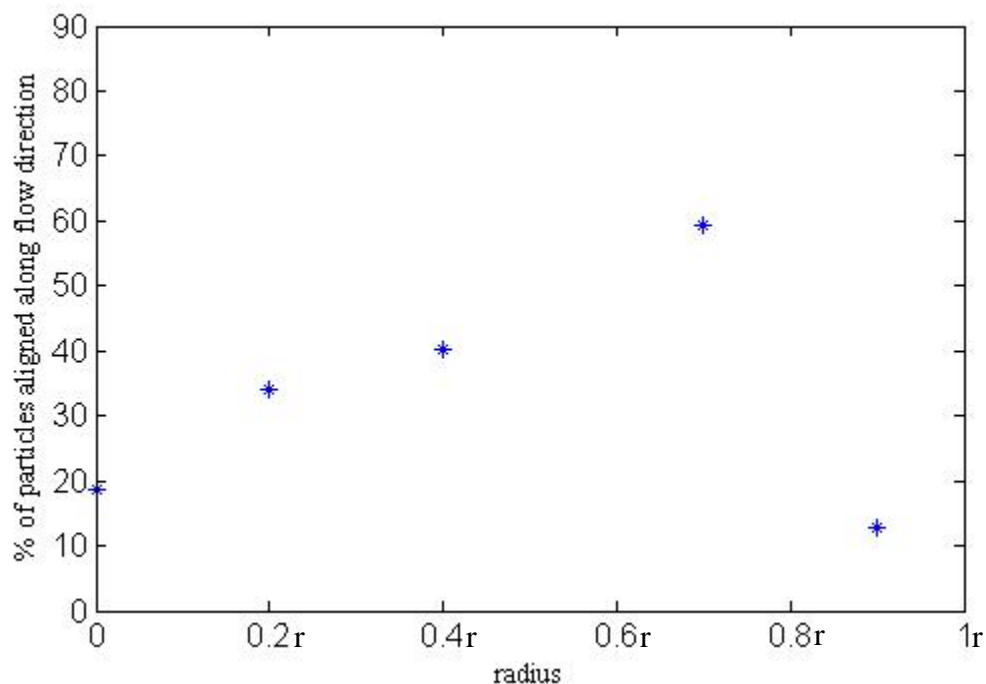


Figure 7.1.1: Effect of radial position on the percentage of particles aligned along flow direction.

The alignment effect is not present at the edge of the wafer; the particles seem to be stacked into a thicker film at the rim of the wafer. From Figure 7.1.1 it is evident that high shear due to the spinning has no effect on the near edge particles. A more complex process is involved at the edge of the wafer. Edge effect is due to the “edge beads” phenomenon which depends on fluid coating properties such as surface tension, viscosity, and spin speed. When the circular wafer rotates in its plane, it behaves like a centrifugal pump¹⁴. It induces a continuous air flow toward the wafer and creates rotational motion at the liquid-air interface. This had been studied by Cochran¹⁵ and Schlichting¹⁶. Due to the centrifugation, as the fluid flows (uniformly) radially outward, the surface tension makes

it difficult to detach from the edge of the wafer. So the fluid remains attached around the perimeter as a “bead”, which is responsible for thicker coating in these areas. This is essentially fluid “pile up” effect with somewhat evaporation drying because of the air flow. Luurtsema¹⁷ discussed the edge effect for rectangular substrates in details. The schematic of the edge effect is shown in Figure 7.1.2.

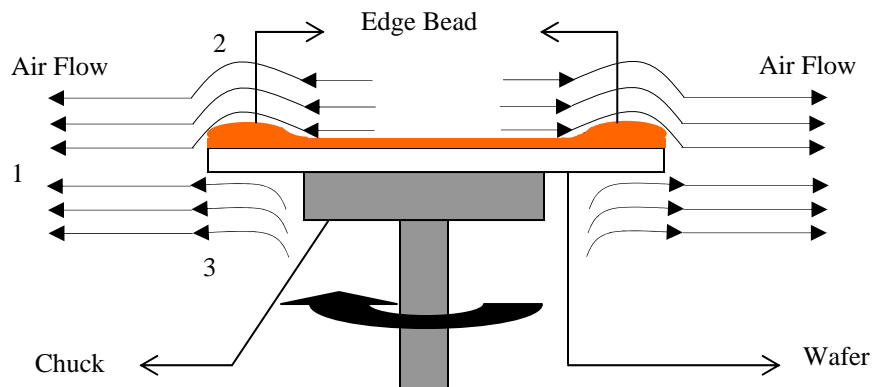


Figure 7.1.2: Schematic of the edge effect.

7.2 Conclusion

In the present work, we showed that cumulative shear does contribute to the alignment of the particles along the radial flow direction during spin coating. The experimental results are in good agreement with our numerical results. The alignment effect is not present at the edge of the wafer. The high shear due to the spinning has no effect on the near edge particles, a more complex process is involved at the edge of the wafer. Edge effect plays an important role on the alignment of the particles near the edge.

8. References

1. A. G. Emslie, F. T. Bonner and C. G. Peck, "Flow of a viscous liquid on a rotating disk", J. Appl. Phys. 29 (1958) 858.
2. D. Meyerhofer, "Characteristics of resist films produced by spinning", J. Appl. Phys. 49 (1978) 3993.
3. D. P. Birnie, III and M. Manley, "Combined flow and evaporation of fluid on a spinning disk", Phys. Fluids. 9 (1997) 870.
4. B.G. Grasher and D. P. Birnie, III, Thesis "Remainder profiles and Shear Evolution During Spin Coating" (2003).
5. E. K. Franke and D. P. Birnie, III, "Fibre orientation during spin coating of composite solutions", J. Mater. Sci. Lett. 14 (1995) 1807.
6. <http://www.scscoatings.com>
7. <http://www.mse.arizona.edu/faculty/birnie/Coatings/KeyStages.htm>
8. <http://www.zeiss.com>.
9. http://midas.npl.co.uk/midas/content/images/ma52_files/image005.jpg
10. <http://mcff.mtu.edu/acmal/sied500.htm>
11. J.B.Cui, C.P.Daghlian,U.J.Gibson,R.Pusche, P.Geithner and L.Ley, "Low-temperature growth and field emission of ZnO nanowire arrays", J.of Appl. Phys. 97 (2005) 044315.
12. B.Poudel,W. Z. Wang, C Dames, J. Y. Huang, S Kunwar, D. Z. Wang, D. Banerjee, G. Chen and Z.F. Ren, "Formation of crystallized titania nanotubes and their transformation into nanowires", Nanotechnology 16(2005) 1935.

13. J.N.Nian and H. Teng, "Hydrothermal synthesis of single-crystalline anatase TiO₂ nanorods as the precursor", J. Phys. Chem. B 110 (2006) 4193.
14. S. Middleman, "The effect of induced air-flow on the spin coating of viscous liquids", J. Appl. Phys. 62 (1987) 2530.
15. W.G. Cochran, "The flow due to a rotating disc", Proc. Cambridge Philos. Soc. 30, (1934) 365.
16. M. Schlichting, Boundary Layer Theory (McGraw-Hill, New York, 1960).
17. G. A. Luurtsema, Thesis "Spin Coating For Rectangular Substrates" (1997).

APPENDIX A

I. Program for Shear Contour Calculation

II. Program for Position Tracking of the Particles During Spin Coating Process

III. Program for Histogram Plotting of Particle Alignment

I. Program for Shear Contour Calculation

```

% 2000 RPM - fluid is ethanol %

k3=9619497467;

% initial height is 100 microns at time zero

h0=0.0001;

t(1)=0.0;

% Hf= 10 micron=0.00001 m %

% Hf=Hcrossover(for evaporation)=0.000003731 m

% tf=1.7 sec %

% Fluid height,z,r for position tracking %

% this loop will control FINAL fluid height %

for k=1:1:9

    z(300)=k*0.000000413;

    %z(300)=k*0.000000322;

    % z(300)=k*0.000001;

    %z(300)=k*0.0000001;

    H(300)=0.000003;

    % t(300)=2.885;

    %t(300)=25.986;

    % t(300)=1.7;

    t(300)=1.864370194;

    % t(300)=30.0;

    % this loop will control FINAL radius location of fluid element

```

```

for l=1:1:9

    r(300)=l*0.01;

    ra(k,l)=r(300);

    zh(k,l)=z(300);

    % Differentiation of Vz & Vr for z & r value repectively %

    % trying to increment time backwards %

    for i=299:-1:1

        h(i)=1.864370194/300;

        K1(i)=h(i)*(k3*z(i+1)^3-(3*h0*k3*z(i+1)^2/sqrt(1+4*k3*h0^2*t(i+1))));

        t1=t(i+1)+h(i)/2;

        Z1=z(i+1)+K1(i)/2;

        K2(i)=h(i)*(k3*Z1^3-(3*h0*k3*Z1^2/sqrt(1+4*k3*h0^2*t1)));

        t2=t(i+1)+h(i)/2;

        Z2=z(i+1)+K2(i)/2;

        K3(i)=h(i)*(k3*Z2^3-(3*h0*k3*Z2^2/sqrt(1+4*k3*h0^2*t2)));

        t3=t(i+1)+h(i);

        Z3=z(i+1)+K3(i);

        K4(i)=h(i)*(k3*Z3^3-(3*h0*k3*Z3^2/sqrt(1+4*k3*h0^2*t3)));

        D(i)=1/6*(K1(i)+2*K2(i)+2*K3(i)+K4(i));

        L(i)=(3*k3*r(i+1)*z(i+1)*h0/sqrt(1+4*k3*h0^2*t(i+1)));

        R1(i)=h(i)*(L(i)-1.5*k3*r(i+1)*z(i+1)^2);

        j1=r(i+1)+R1(i)/2;

        Rd=(3*k3*j1*z(i+1)*h0/sqrt(1+4*k3*h0^2*t1));

```

```

R2(i)=h(i)*(Rd-1.5*k3*j1*z(i+1)^2);
j2=r(i+1)+R2(i)/2;
Rd1=(3*k3*j2*z(i+1)*h0/sqrt(1+4*k3*h0^2*t2));
R3(i)=h(i)*(Rd1-1.5*k3*j2*z(i+1)^2);
j3=r(i+1)+R3(i);
Rd2=(3*k3*j3*z(i+1)*h0/sqrt(1+4*k3*h0^2*t3));
R4(i)=h(i)*(Rd2-1.5*k3*j3*z(i+1)^2);
Dr(i)=1/6*(R1(i)+2*R2(i)+2*R3(i)+R4(i));
z(i)=z(i+1)-D(i);
t(i)=t(i+1)-h(i);
r(i)=r(i+1)-Dr(i);
H(i)=h0/sqrt(1+4*k3*h0^2*t(i));
end;
% shear calculation here %
for ii=1:1:300
T(ii)=3*k3*H(ii)*(r(ii)-2*z(ii));
Tz2(ii)=T(ii)-3*k3*z(ii)*(r(ii)-z(ii));
end;
h0=0.0001;
% Integration %
h1=1.864370194/300;
C1=Tz2(1)+Tz2(300);
for ij=2:2:298

```

```

    Tz(ij)=4*Tz2(ij);

end;

for ik=3:2:299

    Tz11(ik)=2*Tz2(ik);

end;

C2=sum(Tz);

C21=sum(Tz11);

C3(k,l)=h1/3*(C1+C2+C21);

end;

end;

xlswrite('ShearIntegration',C3);

xlswrite('zh',zh);

xlswrite('ra',ra);

% do the shear integration and put result in matrix element%

% mesh(zh,ra,C3,'EdgeColor','black')

% ylim([0 0.1]);

% plot(ra,zh);

% xlim([0 0.1]);

[C,h] = contour(ra,zh,C3);

set(h,'ShowText','on','TextStep',get(h,'LevelStep')*2)

colormap cool

% plot(t,r);

```

II. Program for Position Tracking of The Particles During Spin Coating Process

```

% 2000 RPM - fluid is ethanol %

k3=9619497467;

% initial height is 100 microns at time zero

h0=0.0001;

t(1)=0.0;

% Hf= 10 micron=0.00001 m %

% Hf=Hcrossover(for evaporation)=0.000003731 m

% tf=1.7 sec %

% Fluid height,z,r for position tracking %

% this loop will control FINAL fluid height %

for k=9:-1:1

    l=9-(k-1);

    z(1)=k*0.000000413;

    %z(1)=0.000000372;

    %z(300)=k*0.000000322;

    % z(300)=k*0.000001;

    %z(300)=k*0.0000001;

    H(1)=0.0001;

    % t(300)=2.885;

    %t(300)=25.986;

    % t(300)=1.7;

    %t(300)=1.864370194;

```

```

% this loop will control FINAL radius location of fluid element

r(1)=l*0.01;

ra(1,k)=r(1);

zh(1,k)=z(1);

% Differentiation of Vz & Vr for z & r value repectively %

% trying to increment time backwards %

for i=2:1:300

    h(i)=30/300;

    K1(i)=h(i)*(k3*z(i-1)^3-(3*h0*k3*z(i-1)^2/sqrt(1+4*k3*h0^2*t(i-1))));

    t1=t(i-1)+h(i)/2;

    Z1=z(i-1)+K1(i)/2;

    K2(i)=h(i)*(k3*Z1^3-(3*h0*k3*Z1^2/sqrt(1+4*k3*h0^2*t1)));

    t2=t(i-1)+h(i)/2;

    Z2=z(i-1)+K2(i)/2;

    K3(i)=h(i)*(k3*Z2^3-(3*h0*k3*Z2^2/sqrt(1+4*k3*h0^2*t2)));

    t3=t(i-1)+h(i);

    Z3=z(i-1)+K3(i);

    K4(i)=h(i)*(k3*Z3^3-(3*h0*k3*Z3^2/sqrt(1+4*k3*h0^2*t3)));

    D(i)=1/6*(K1(i)+2*K2(i)+2*K3(i)+K4(i));

    L(i)=(3*k3*r(i-1)*z(i-1)*h0/sqrt(1+4*k3*h0^2*t(i-1)));

    R1(i)=h(i)*(L(i)-1.5*k3*r(i-1)*z(i-1)^2);

    j1=r(i-1)+R1(i)/2;

    Rd=(3*k3*j1*z(i-1)*h0/sqrt(1+4*k3*h0^2*t1));

```

```

R2(i)=h(i)*(Rd-1.5*k3*j1*z(i-1)^2);
j2=r(i-1)+R2(i)/2;
Rd1=(3*k3*j2*z(i-1)*h0/sqrt(1+4*k3*h0^2*t2));
R3(i)=h(i)*(Rd1-1.5*k3*j2*z(i-1)^2);
j3=r(i-1)+R3(i);
Rd2=(3*k3*j3*z(i-1)*h0/sqrt(1+4*k3*h0^2*t3));
R4(i)=h(i)*(Rd2-1.5*k3*j3*z(i-1)^2);
Dr(i)=1/6*(R1(i)+2*R2(i)+2*R3(i)+R4(i));
z(i)=z(i-1)+D(i);
t(i)=t(i-1)+h(i);
r(i)=r(i-1)+Dr(i);
H(i)=h0/sqrt(1+4*k3*h0^2*t(i));
ra(i,k)=r(i);
zh(i,k)=z(i);

end;

% shear calculation here %

for ii=1:1:300

T(ii)=3*k3*H(ii)*(r(ii)-2*z(ii));

Tz2(ii)=T(ii)-3*k3*z(ii)*(r(ii)-z(ii));

end;

end;

% xlswrite('ShearIntegration',C3);

% xlswrite('zh',zh);

```

```
%xlswrite('ra',ra);  
  
% do the shear integration and put result in matrix element%  
  
%mesh(zh,ra,C3,'EdgeColor','black')  
  
%ylim([0 0.1]);  
  
%[C,h] = contour(ra,zh,C3);  
  
%set(h,'ShowText','on','TextStep',get(h,'LevelStep')*2)  
  
%colormap cool  
  
plot(ra,zh);  
  
xlim([0 0.1]);
```

III. Program for Histogram Plotting of Particle Alignment

```
An=data(:,1);  
  
Ar=data(:,2);  
  
N=118;  
  
k=0;  
  
M=0;  
  
L1=0;  
  
L2=0;  
  
L3=0;  
  
L4=0;  
  
L5=0;  
  
L6=0;  
  
L7=0;  
  
L8=0;
```

```
L9=0;
L10=0;
L11=0;
L12=0;
for i=1:1:N
    if(Ar(i)>2.5 & Ar(i)<5.5)
        k=k+1;
        AR(k)=Ar(i);
        AN(k)=An(i);
        if(AN(k)<15.0 )
            L1=L1+1;
        elseif(AN(k)>15.0& AN(k)<30.0)
            L2=L2+1
        elseif(AN(k)>30.0& AN(k)<45.0)
            L3=L3+1;
        elseif(AN(k)>45.0 & AN(k)<60.0)
            L4=L4+1;
        elseif(AN(k)>60.0 & AN(k)<75.0)
            L5=L5+1;
        elseif(AN(k)>75.0 & AN(k)<90.0)
            L6=L6+1;
        M=M+1;
        elseif(AN(k)>90.0 & AN(k)<105.0)
```

```
L7=L7+1;
elseif(AN(k)>105.0 & AN(k)<120.0)
    L8=L8+1;
elseif(AN(k)>120.0 & AN(k)<135.0)
    L9=L9+1;
elseif(AN(k)>135.0 & AN(k)<150.0)
    L10=L10+1;
elseif(AN(k)>150.0 & AN(k)<165.0)
    L11=L11+1;
elseif(AN(k)>165.0 & AN(k)<180.0)
    L12=L12+1;
else
    end;
else
    end;
end;
l=15:15:180;
n(1)=L1;
n(2)=L2;
n(3)=L3;
n(4)=L4;
n(5)=L5;
n(6)=L6;
```

n(7)=L7;

n(8)=L8;

n(9)=L9;

n(10)=L10;

n(11)=L11;

n(12)=L12;

bar(l,n);

xlabel('Angle of Alignment');

ylabel('No of Particles');